

Civil Engineering Journal

(E-ISSN: 2476-3055; ISSN: 2676-6957)

Vol. 11, No. 09, September, 2025



Finite Element Analysis on Shear Responses of Reinforced Concrete Beams Strengthened with ETS-FRP Bars

Linh Van Hong Bui ^{1, 2}, Boonchai Stitmannaithum ^{3*}

¹ Faculty of Civil Engineering, Ho Chi Minh City University of Technology (HCMUT), Ho Chi Minh City, Vietnam.

² Vietnam National University Ho Chi Minh City (VNU-HCM), Ho Chi Minh City, Vietnam.

Received 17 June 2025; Revised 19 August 2025; Accepted 26 August 2025; Published 01 September 2025

Abstract

This study conducts a numerical analysis on the shear performance of reinforced concrete beams retrofitted with fiber-reinforced polymer (FRP) bars with embedded through-section (ETS) technique. The study uses 3D nonlinear finite element method (FEM) and evaluates the shear features of ETS-FRP-strengthened beams in failure modes, shear capacity, stiffness, and ductility. The FE analyses consider the effects of key design parameters, including transverse steel stiffness ($E_{SW}\rho_{SW}$), ETS-FRP bar stiffness (E_{fPf}), compressive strength of concrete (f^*c), beam geometry, and the values of shear span-to-effective depth (a/d) ratio. Consequently, ETS-strengthened beams with higher concrete strength (f^*c) or greater total rigidity of ETS and transverse reinforcement ($E_{fPf} + E_{SW}\rho_{SW}$) showed notable improvements in stiffness and load-carrying capacity, with average increases exceeding 20%. The enhancement in shear strength from increased shear reinforcement stiffness is less pronounced in specimens with high concrete strength than in those with lower strength. ETS-strengthened beams with T-shaped sections exhibit more effective performance and safer failure modes. An enhancement in the a/d ratio reduces the stress in ETS bars but results in more ductile failures. This study also proposes a new analytical formulation for determining the maximum shear resistance of ETS-intervened beams, accounting for all failure modes. The model achieved an average predicted-to-tested shear maximum force ratio of 0.93 along with a coefficient of variation of 26%, demonstrating improved accuracy compared to existing models.

Keywords: Embedded Through-Section; FRP; Finite Element Analysis; Shear Behavior; Shear Strength Model.

1. Introduction

In recent years, a novel strengthening technique, namely deep embedment or embedded through-section (ETS) method, has been created to enhance the performance of reinforced concrete (RC) beams. This method strategically integrates the advantages and addresses the key limitations of existing near-surface mounted (NSM) and externally bonded (EB) retrofitting approaches, as reported in the literature [1–3]. In both EB and NSM techniques, steel or fiber-reinforced polymer (FRP) composites are externally applied to pre-treated concrete surfaces at critical beam zones [4–6]. Numerous studies [7–12] have demonstrated that these techniques can significantly improve the beam capacity and stiffness. However, EB and NSM methods are not without challenges. Two of the most critical drawbacks are the premature debonding of strengthening FRP elements from the concrete and the rapid degradation of FRP performance—especially its bonding effectiveness—under elevated temperatures or fire exposure [13, 14]. The ETS method has emerged as a promising alternative to overcome these issues.

^{*} Corresponding author: boonchai.s@chula.ac.th





© 2025 by the authors. Licensee C.E.J, Tehran, Iran. This article is an open access article distributed under the terms and conditions of the Creative Commons Attribution (CC-BY) license (http://creativecommons.org/licenses/by/4.0/).

³ Center of Excellence in Innovative Construction Materials, Department of Civil Engineering, Faculty of Engineering, Chulalongkorn University, Bangkok, Thailand.

The ETS method employs the FRP or steel bars (or even any configurations such as fibers and laminates that can go through the holes), which are vertically or diagonally inserted into the prefabricated holes through the center of member section [3, 13–18]. Several studies [14–17] indicated that the contribution of the ETS system for shear intervention of RC beams are drastically greater than that of the NSM and EB methods for retrofiting of RC beams. The improved fire resistance and mitigation of early debonding in ETS-FRP strengthened RC beams deem to be largely attributed to the effective confinement of the ETS bars within the concrete core. This inherent confinement not only provides mechanical protection to the FRP bars but also significantly reduces their exposure to elevated temperatures, which typically degrade the bonding performance in externally bonded systems. Moreover, the concrete cover acts as a thermal barrier, enhancing the durability of the retrofit under fire conditions.

In addition to confinement, the use of anchoring nuts at the ends of the ETS bars presents a practical and robust solution to fully exploit the tensile capacity of the FRP reinforcement. Such anchorage systems help transfer stresses more efficiently between the FRP rods and concrete, reducing the risk of premature loss of adhesion. Together, these features contribute to a more reliable and durable strengthening technique, addressing critical limitations observed in conventional EB and NSM methods [14]. Despite the promising potential of the ETS strengthening method, existing research on RC beams reinforced using this technique remains limited. Critical variables that fundamentally influence the shear performance—such as the stiffness contribution from ETS bars $(E_{IP}f)$ and transverse steel reinforcement $(E_{SW}\rho_{SW})$, variations in concrete strength (f'c), diverse beam geometries, and the values of the shear span-to-effective depth (a/d) ratio—have not been comprehensively investigated. This lack of systematic study on these parameters creates a significant knowledge gap in fully understanding and optimizing the ETS strengthening system for practical applications. Addressing these variables is essential for developing reliable design guidelines and predictive models that can accurately capture the complex interactions governing the responses of ETS-strengthened beams subjected to shear action.

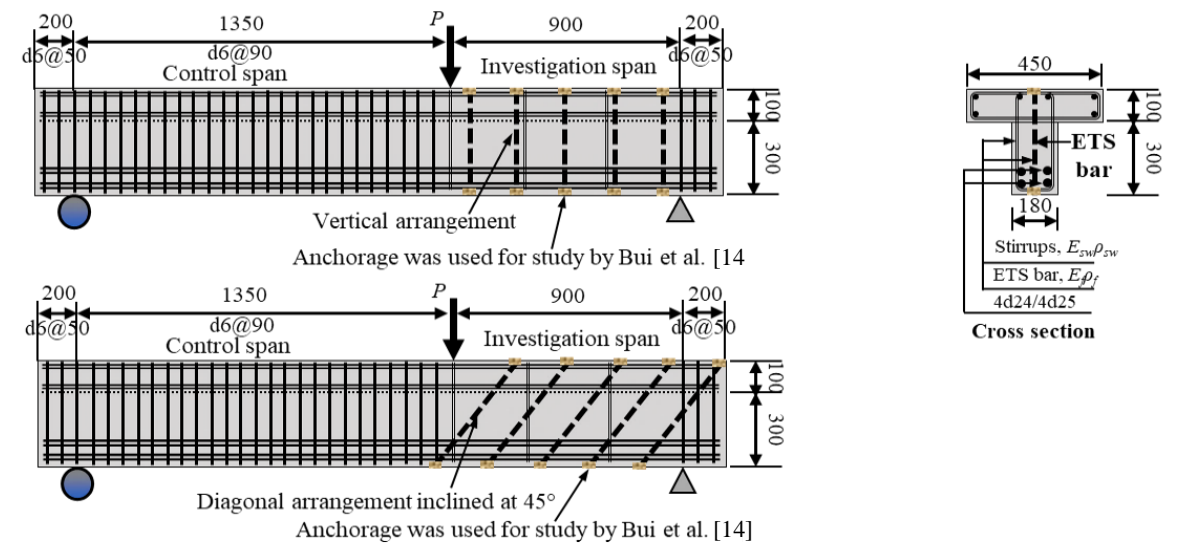
The finite element method (FEM) has been applied to analyze the shear properties of the ETS-FRP-strengthened RC in some numerical research [18–22]. The reliability of the FE models developed in their studies has been verified on the wide analyses of the beam shear behaviors in comparison with the available test data. Thus, the FEM simulation is helpful for investigating the shear characteristics of the ETS-intervened beams under crucial design variables, which have never examined in any previous studies. Bui et al. [14] indicated that the calculations of shear resistance of ETS-retrofitted beams and contribution in shear of ETS retrofitting elements made by the equations of the American Concrete Institute (ACI), ACI 318-19 [23] and ACI 440.1R-15 [24], and the Japanese Society for Civil Engineers (JSCE), JSCE 2007 [25], provided the conservative predictions. The applicability of the shear strength approaches in those guidelines for the ETS-intervened RC beams remains a challenge.

This study provides new insights into the shear behavior of RC beams intervened with ETS rods through numerical investigations using FEM simulations in ANSYS software [26]. First, the reliability of the FEM simulation is validated against available experimental results. Then, extensive parametric analyses are performed to examine the effects of key variables on beam behavior, including the total reinforcement stiffness ($E_{sw}\rho_{sw} + E_{f}\rho_{f}$) by varying the stiffness ratio ($E_{f}\rho_{f}/E_{sw}\rho_{sw}$), concrete compressive strength (f'_{c}) at 20 MPa, 38 MPa, and 70 MPa, beam geometry with rectangular and T-shaped sections, and the shear span over effective depth ratio (a/d). Alongside model validation, experimental results from previous studies are employed to verify and analyze the outcomes of these parametric investigations. Furthermore, the applicability of existing shear strength models from current guidelines [23–25] is assessed for ETS-strengthened beams and ETS-FRP bars. Based on these analyses, a new empirical shear capacity formulation specifically for ETS-retrofitted beams is proposed.

2. Specimen Configurations and Specifications

Figure 1 presents the detail configurations and specifications of the ETS-strengthened beams. Three experimental studies regarding the ETS-intervened beams by Mofidi et al. [16], Breveglieri et al. [17], and Bui et al. [14] are considered. As schemed by Figure 1, in the experiments of Bui et al. [14] and Breveglieri et al. [17], the ETS strengthening systems in the beams B2, B4, C2, and C4 were inclined at 45°, while the remaining specimens had vertical ETS strengthening bars. In fact, the reliability of FEM for forecasting the shear features of ETS-FRP-intervened RC beams has been proven in few studies [18–21]. Breveglieri et al. [18] used the smeared crack approach for the 2D FE models, while the works by Bui et al. [19, 20, 21] and Godat et al. [22] employed the commercial packages for the 3D FEM simulations. In Section 3, an attempt is made to further validate the FE models made of ANSYS software [26] for two beams C1 and C2 in the literature by Breveglieri et al. [17], which were investigated in a previous study by the authors of the present work [21]. However, the numerical investigation toward the validation of the FE models of the foregoing two beams (C1 and C2) remains shallow. Aside from Figure 1, Table 1 depicts the necessary information of the specimens in the past experiments and the parametric study. More details of the beams in the tests could be found in the reference studies [14–17]. All beam data of the previous experimental works and parametric studies provided in Table 1 are employed to conduct the assessment of the shear capacity models in Section 5.

Beam configurations in studies by Breveglieri et al. [17], Bui et al. [14], and for parametric study



Beam configurations in study by Mofidi et al. [16]

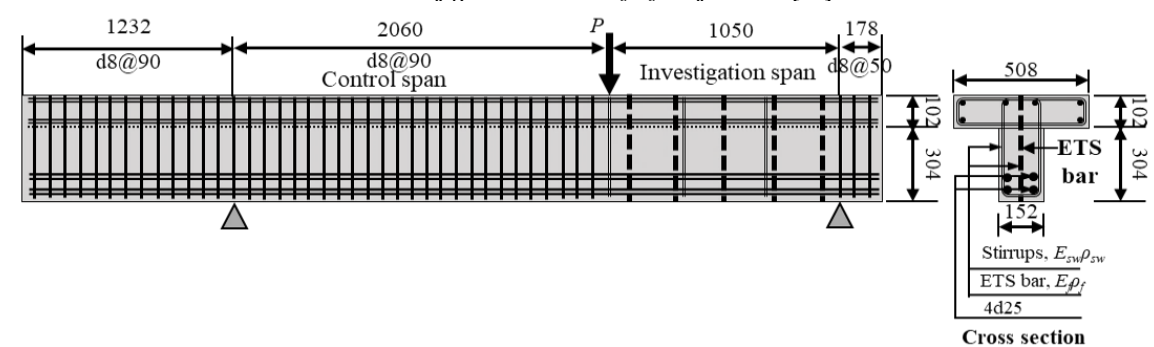


Figure 1. Configurations of beams (dimensions in mm) [14-17]

Table 1. Details of beams from previous studies [14-17] and those designed for the parametric study

Study	Beams	$ ho_{sw}$ $(\%)$	Esw (GPa)	<i>dsw</i> (mm)	<i>d_f</i> (mm)	ρ _f (%)	E _f (GPa)	f_c '(MPa)	f _f (MPa)	$E_f ho_f / E_{sw} ho_{sw}$	$E_f \rho_f + E_{sw} \rho_{sw} $ (MPa)
					Experim	ental wor	ks				
	B1	0.11	200	6	10	0.24	50	38	1076	0.551	341.2
Bui et al. [14]	B2	0.11	200	6	10	0.34	50	38	1076	0.779	391.4
Bui et al. [14]	В3	0.24	200	9	10	0.24	50	38	1076	0.253	601.2
	B4	0.24	200	9	10	0.34	50	38	1076	0.357	651.4
	C1	0.11	200	6	8	0.16	160	29.7	1920	1.128	468
Breveglieri et al.	C2	0.11	200	6	8	0.22	160	29.7	1920	1.596	571
[17]	C3	0.17	200	6	8	0.16	160	29.7	1920	0.517	588
	C4	0.17	200	6	8	0.22	160	29.7	1920	0.731	729
	D1	-	-	8	12.7	0.64	148	29.6	2800	-	1021
	D2	0.38	200	8	9.5	0.18	148	29.6	2800	0.349	1044
	D3	0.38	200	8	12.7	0.32	148	29.6	2800	0.624	1268
Mofidi et al. [16]	D4	0.38	200	8	12.7	0.64	148	25	2800	1.248	1776
	D5	0.38	200	8	9.5	0.18	148	29.6	2800	0.349	1058
	D6	0.25	200	8	12.7	0.64	148	29.6	2800	1.898	1516

Study	Beams	$ ho_{sw}$ $(\%)$	Esw (GPa)	<i>dsw</i> (mm)	<i>d_f</i> (mm)	ρ _f (%)	E _f (GPa)	f_c '(MPa)	f _f (MPa)	$E_f ho_f / E_{sw} ho_{sw}$	$E_f \rho_f + E_{sw} \rho_{sw} $ (MPa)
	Parametr	ic studies	on effects o	f the concre	ete strengtl	h, the stif	fness of or	dinary steel st	irrups and	d ETS bars	
	G0_B0	0.09	200	6	10	0.15	75	20	1366	0.564	302.4
	G0_B1	0.10	200	6	10	0.10	120	20	1700	0.556	325.8
	G0_B2	0.14	200	6	10	0.29	40	20	755	0.417	395.6
Group 0	G0_B3	0.19	200	10	8	0.06	200	20	-	0.320	512.0
	G0_B4	0.24	200	9	10	0.24	50	20	1076	0.257	592.4
	G0_B5	0.31	200	9	9.5	0.13	100	20	1500	0.209	759.6
	G0_B6	0.39	200	9	9	0.08	160	20	2400	0.160	911.1
	G1_B0	0.09	200	6	10	0.15	75	38	1366	0.564	302.4
	G1_B1	0.10	200	6	10	0.10	120	38	1700	0.556	325.8
	G1_B2	0.14	200	6	10	0.29	40	38	755	0.417	395.6
Group 1	G1_B3	0.19	200	10	8	0.06	200	38	-	0.320	512.0
	G1_B4	0.24	200	9	10	0.24	50	38	1076	0.257	592.4
	G1_B5	0.31	200	9	9.5	0.13	100	38	1500	0.209	759.6
	G1_B6	0.39	200	9	9	0.08	160	38	2400	0.160	911.1
	G2_B0	0.09	200	6	10	0.15	75	70	1366	0.564	302.4
	G2_B1	0.10	200	6	10	0.10	120	70	1700	0.556	325.8
	G2_B2	0.14	200	6	10	0.29	40	70	755	0.417	395.6
Group 2	G2_B3	0.19	200	10	8	0.06	200	70	-	0.320	512.0
•	G2_B4	0.24	200	9	10	0.24	50	70	1076	0.257	592.4
	G2 B5	0.31	200	9	9.5	0.13	100	70	1500	0.209	759.6
	G2_B6	0.39	200	9	9	0.08	160	70	2400	0.160	911.1

Notes: E_{sw} is the modulus of elasticity of transverse steel (GPa); ρ_{sw} is the percentage of steel stirrups (%); d_{sw} is the diameter of ordinary stirrups (mm); E_f is the ETS elastic modulus (GPa); ρ_f is the percentage of ETS rods (%); d_f is the diameter of ETS rods (mm); f'_c is the strength of concrete due to compression (MPa).

The specimens are aimed to collapse in shear at the span with ETS intervening elements, in which the control shear span and flexural bending are over-reinforced. For FEM validation to the experimental study by Breveglieri et al. [17], the yielding stress levels of the steel reinforcing rods with 6 and 24 mm diameter were 574 and 598 MPa, respectively. The FE analyses of the parametric studies use the Thai Industrial Standards (TIS20-2543 [27] and TIS24-2548 [28]) for determining the yielding stress levels of the steel rods with 6 mm, 9 mm, and 25 mm diameters that are 235, 235, and 390 MPa, respectively. The modulus of elasticity of the steel reinforcing bars is assumed by 200 GPa for all specimens. The design variables for the parametric studies in this work are the concrete strength due to compression (f^{*}_c), the stiffness of the reinforcing steel ($E_{SW}\rho_{SW}$) and ETS strengthening bars (E_{IPf}), beam geometry, and a/d ratio.

For the first three variables (f'_c , $E_{sw}\rho_{sw}$, $E_f\rho_f$), the beams are designed and categorized into three groups which are G0, G1, and G2, as presented in Table 1. The geometries of the beams in groups G0, G1, and G2 are the same with the beam dimensions in the study by Bui et al. [14], as illustrated in Figure 1. In order to represent three typical levels of low concrete strength, normal concrete strength, and high concrete strength, specimens in G0, G1, and G2 have different values of concrete compressive strengths of 20, 38, and 70 MPa, respectively. Each group consists of seven specimens (B0–B6), and the specimen's names are ordered to have the increase of the total stiffness ($E_f\rho_f + E_{sw}\rho_{sw}$) by decreasing the stiffness ratio ($E_f\rho_f/E_{sw}\rho_{sw}$). This condition is to consider the unified assessment on the design parameters regarding the shear reinforcement and strengthening stiffnesses. Consider the effectiveness for practical use, all beams are designed so that the steel shear reinforcement reaches the yielding stage at failure. Conversely, for the variable of member geometry and a/d values, the details of the beams are provided later in Section 4.3.

3. Finite Element Method

The information for the FE models using the available commercial package of ANSYS software [26], which is common in the structural engineering community, are presented in this section. The validation of the FE models for two beams C1 and C2, which were tested in the experimental program by Breveglieri et al. [17], is made in this section. The ETS strengthening bars in the beam C1 were placed with the vertical inclination while the beam C2 had diagonal ETS strengthening system. After verifying the rationale of the FEM simulation, a FE model is extended to implement the parametric studies in Section 4.

3.1. Elements and Material Laws

ANSYS package [26] has been used to establish 3D FE models of the beams intervened in shear with ETS rods. The elements LINK180, SOLID65, and SOLID45 in the library of ANSYS [26] are adopted to model the mechanical responses of the steel or FRP rods, concrete, and supporting or loading rigid plates, respectively [19, 20]. The SOLID65 element consists of eight nodes. The material constitutive models proposed by Hognestad et al. [29] (Equation 1) and Willam & Warnke [30] are used to describe the concrete subjected to compression and tension as shown in Figures 2-a and 2-b, respectively. In Figure 2-b, f'_{ct} is the concrete tensile cracking capacity taken by $0.6\sqrt{f'_c}$ (MPa) [22]. The plasticity behavior of concrete uses the material model option by kinematic isotropic hardening. The smeared approach for simulating the cracking mechanism of concrete material is used. The Poisson's ratio for concrete is 0.2.

$$f_c = f_c' \left[2 \left(\frac{\varepsilon}{\varepsilon_0} \right) - \left(\frac{\varepsilon}{\varepsilon_0} \right)^2 \right] \tag{1}$$

where f_c denotes the stress in concrete under compression process (MPa) corresponding to the specific strain ε ; f'_c is the peak concrete strength under compression (MPa); $\varepsilon_0 = 2f'_c/E_c$ (μ m/m), and $E_c = 3300\sqrt{f'_c} + 6900$ refers to the modulus of elasticity of the concrete (MPa) [21]; $\varepsilon_u = 0.0038$ refers to the ultimate strain of concrete at stage of crushing.

Shear transfer coefficients are used to quantify the degree of shear stress transmitted across cracks, distinguishing between open and closed crack conditions. These coefficients typically range from 0.0 to 1.0, where a value of 0.0 indicates no shear transfer (smooth crack surface), and 1.0 reflects complete shear transfer (rough or interlocked crack surface). The amount of shear that can be transmitted across a crack increases with higher coefficient values. Previous studies have not established standard values for these parameters due to variations in failure mechanisms and solution convergence issues. In the case of ETS-strengthened beams, substantial shear transfer is expected as the embedded bars span the entire cross-section, facilitating an arch—tie interaction. Based on a series of finite element simulations using various shear transfer values and comparisons with experimental data, this study recommends using 0.5 for open cracks and 1.0 for closed cracks to achieve accurate and stable modeling results.

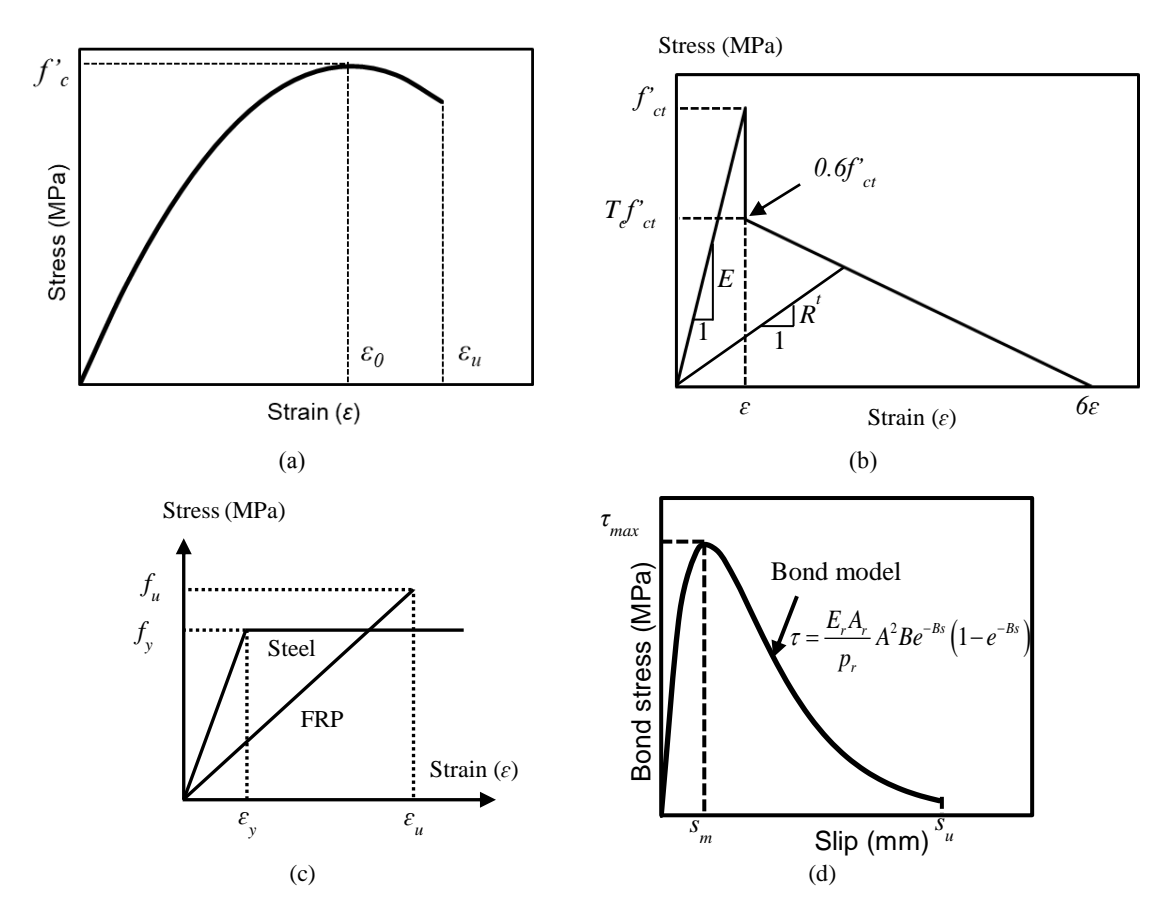


Figure 2. Material property modeling approaches [20]: (a) compressive behavior of concrete; (b) tensile behavior of concrete; (c) constitutive models for steel and FRP bars; (d) bond-slip relationship between reinforcement and concrete

The material rules for steel reinforcement and FRP elements are described in Figure 2-c. The elastoplastic trend is assumed for the steel, while the idealized linear trend until rupture is assumed for mechanical response of the FRP rods. The properties of the steel reinforcement and FRP bars for each specimen are shown in Table 1. The Poisson's ratios for steel reinforcing bars and FRP elements in the FE analyses are 0.3 and 0.28, respectively. The interfacial bond-slip model for the ETS-FRP bars-concrete and steel-concrete contacts proposed in the study by Bui et al. [20] is shown as

$$\tau = A^2 B \frac{E_r A_r}{p_r} e^{-BS} (1 - e^{-BS}) \tag{2}$$

where τ denotes the interfacial bond stress (MPa); A and B represents the bond factors; E_r , A_r , and p_r are the modulus of elasticity of ETS rod or steel reinforcing bar (GPa), the cross-section area of ETS or steel bar (mm²), and the periemeter of the ETS or steel bar (mm), respectively; s denotes the interfacial slip (mm).

The element COMBIN39 represented by non-linear spring model is used to model the interfacial links of ETS bar adherence-concrete and steel-concrete contacts. The τ -s bond model proposed in the study by Bui et al. [20] is formulated in Equation 2 and demonstrated in Figure 2-d. The bond-slip law by Bui et al. [20] includes two key factors A and B. For the ETS bar-concrete bond profile, the values of A and B are used from the suggestion of Bui et al. [20] depending on the average effective bond length. The values of A (\$\varepsilon\$) and B (1/mm) are respectively ranged in 0.0076-0.01468 and 2.59-4.12 for the average effective bond length $(\overline{L_{fi}})$ ranged in 120-150 mm. The A and B values can be determined by linear interpolations on the foregoing data ranges. The average effective bond length $(\overline{L_{fi}})$ is defined as Equation 3-c after the amount of affected ETS rods (Equation 3-a) and the embedded bond length of each affected ETS bars (Equation 3-b) are determined.

$$N_f = \text{round off } \left[h_w \frac{\cot \theta + \cot \alpha}{s_{fw}} \right]$$
 (3-a)

$$N_{f} = \text{round off } \left[h_{w} \frac{\cot \theta + \cot \alpha}{s_{fw}} \right]$$

$$L_{fi} = \begin{cases} i s_{fw} \frac{\sin \theta}{\sin(\theta + \alpha)} & \text{for } x_{fi} < \frac{h_{w}}{2} (\cot \theta + \cot \alpha) \\ L_{f} - i s_{fw} \frac{\sin \theta}{\sin(\theta + \alpha)} & \text{for } x_{fi} \ge \frac{h_{w}}{2} (\cot \theta + \cot \alpha) \end{cases}$$
(3-a)
$$(3-a)$$

$$\overline{L_{fi}} = \frac{1}{N_f} \sum_{i=1}^{N_f} L_{fi} \tag{3-c}$$

where $x_{fi} = is_{fw}$ refers to the length (in mm) from the tip of the primary crack to the endpoint of the *i*th FRP bar that extends beyond the critical crack plane; s_{fw} is the spacing between ETS rods (mm); h_w is the section height of the beams (mm); and θ and α are the diagonal crack angle and the inclination of strengthening systems, respectively (°).

Then, the technique furnished by Bui et al. [20] is adopted to convert the τ -s curves to the force-displacement curves, which are required for load–displacement curves (F_n-D_n) at each element, as follows:

$$F_n = \tau_n \times e_n \times \pi \times d_f \tag{4-a}$$

$$D_n = s_n \tag{4-b}$$

where τ_n = local bond stress at each element defined by Equation 2 (MPa); e_n = the element meshing size of 25 (mm); d_f = the diameter size of ETS rod (mm); s_n = the slip at each element (mm).

Regarding the steel reinforcement–concrete contacts, the interfacial bond factors A and B for τ –s curves are also attained using the technique proposed by Bui et al. [20]. The peak bond stress of $2.5\sqrt{f_c'}$ (MPa) and ultimate slip of 1 (mm) are employed the values provided by fib Model Code 2010 [31].

Figure 3 describes the half 3D FE model of a representative beam associated with an illustration of the bond link for the ETS rod-concrete interfaces via the COMBIN39 element. The components and elements of the beams such as supporting and loading plates, concrete, ETS bars, stirrups, tension steel bars, and compression steel bars are clearly identified. The symmetry boundary conditions at a plane with respect to the geometry, dimensions, constraints, and loading process are assigned. The conditions for the supporting constraints in the FE models are simulated to satisfy the actual tested conditions of the roller and pinned supports. Mesh convergence analysis has been carried out earlier to maximize the accuracy and minimize the computational time. The suitable meshing size of elements is $25 \times 25 \times 25$ mm³. Parallel with the ETS-strengthened RC beams, their corresponding reference beams with no ETS system are simulated to investigate the strengthening efficiency of ETS bars. The displacement control is used for the numerical FE models. In the FEM simulation, failure is characterized by the yielding of steel stirrups, followed either by shearinduced concrete cracking or concrete crushing beneath the loading point. Concrete is deemed to be failed in compression (or 'crushing') when the large area of principal strain exceeds its ultimate strains.

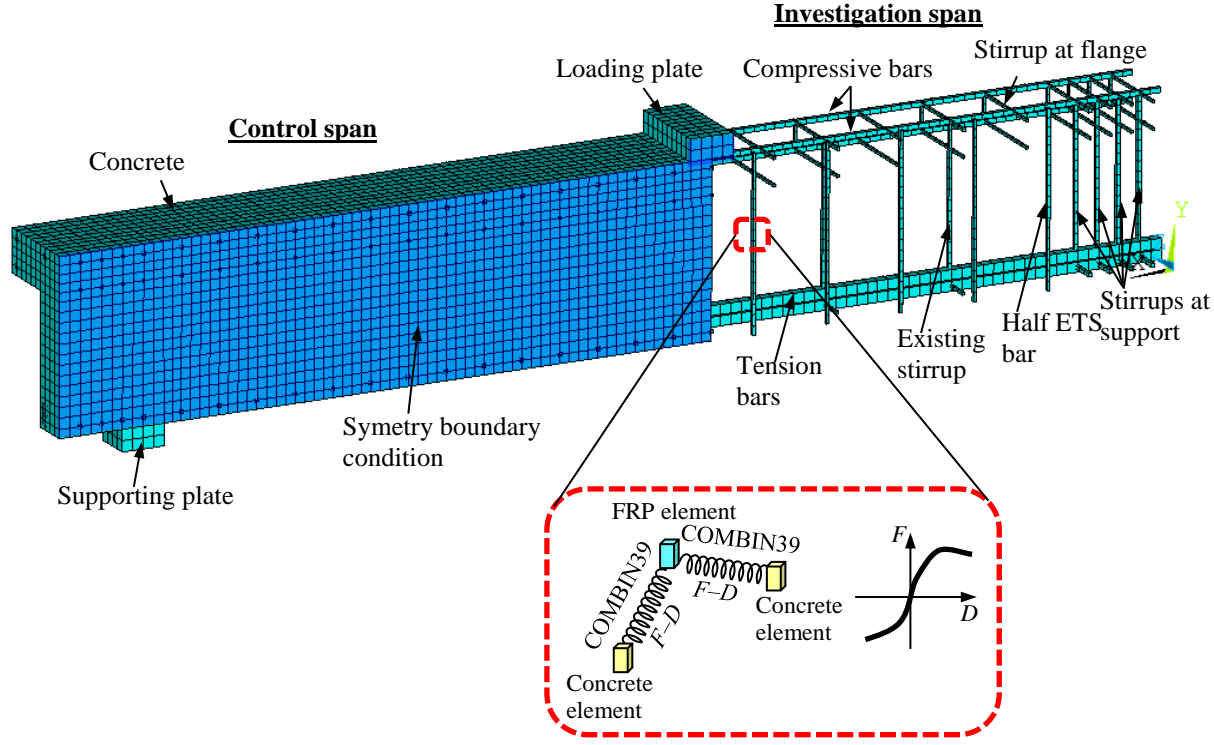


Figure 3. A half 3D FE model with mesh refinement incorporating display of spatial arrangement of reinforcement for a representative specimen

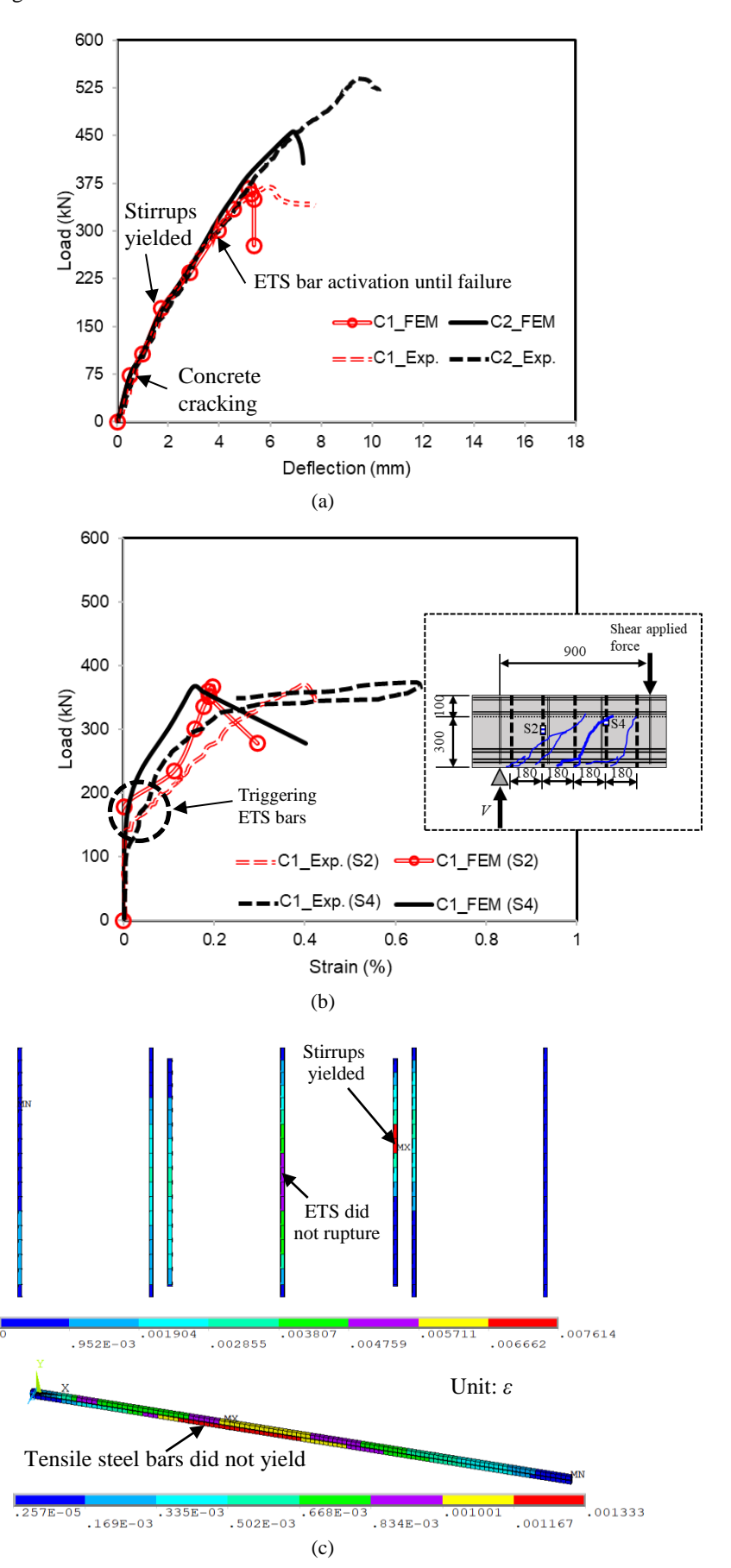
3.2. Verification

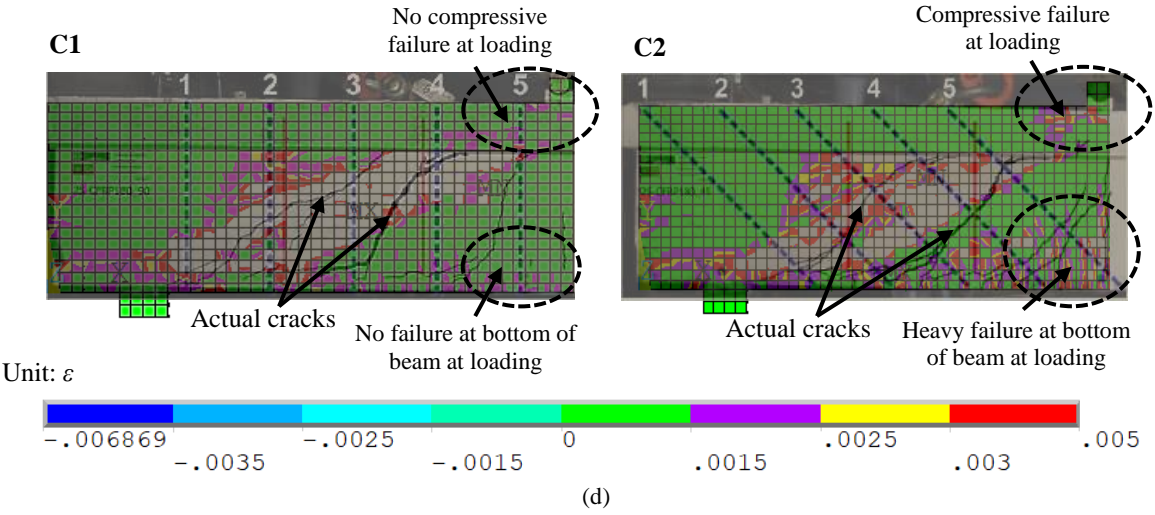
In the past works [18–22], the reasonability of the FE models of the ETS-intervened RC beams has been corroborated considering the validations in the load-bearing capacity, strain in strengthening and reinforcement, and failure mode. However, the numerical validations for the beams retrofitteded with ETS-CFRP bars (C1 and C2) with ANSYS [26] are further required toward the universal application of FEM. This section carefully clarifies the reliability of the FE models against the experiments through deeper analyses. Figure 4-a provides the validation in load-deflection relationships of the ETS-strengthened beams. Apparently, the numerical results via the load-displacement curves agree well with the tested results, particularly in the member stiffness. The differences in the peak loads between FEM simulations and experiments are near 0% for specimen C1 and less than 15% for specimen C2. Further, as indicated in Figure 4-a, three stages of the beam behaviors under the load increase characterized by the FE models strongly agree with those characterized by the tests. Three behavioral stages of an ETS-strengthened beam are concrete cracking, stirrup yielding, and ETS activation until failure. The shear performance of the beam with diagonal inclination of ETS rods is better than that of the beam with vertical ETS bars. This finding can be observed in both simulations and tests. On other hand, the FE models cannot estimate the postpeak behavior of the ETSintervened RC beams. This might be because the experimental test allowed the free deformation until failure, while the FEM simulation was terminated when concrete strain exceeded its ultimate value under a specific increment in displacement. To have the reasonable analyses, this study considers the ascending behavior of the ETS-strengthened beams, which ensures the safety format of the member under critical shear failure.

The stiffness and strength of the beam C1 produced by simulation definitely fit with those monitored by experiment. However, for the beam C2, despite the stiffness made by simulation and experiment is identical, the experimental peak load is higher than numerical maximum load. This could be due to that the specimen C2 had large percentage of ETS bars and long bonded length (via diagonal inclination), providing the great cohesive efficiency for resisting the shear. Meanwhile, in the FEM simulation, the cohesive variables (*A*, *B*) assumed in the bond model for ETS-CFRP barconcrete interface were taken by a linear-interpolation the values obtained from the pull-out tests by Bui et al. [20]. This condition restrains the transferable stress from concrete to ETS-CFRP bars, i.e., limiting the strength development in ETS-CFRP bars for bearing the extent of shear forces.

Figure 4-b presents the corroboration of the FEM model in the strain response in ETS-CFRP bars. Two positions of strain gauges (S2 and S4) in the ETS intervening element of the specimen C1 are considered. Clearly, the strain at cracks (S4) is greater than the strain at S2, which is far from cracks, and this phenomenon is found in both test and simulation. The tendency of strain response can be well captured by the FE models, in which the deformation in ETS bars behaved quasi-linear at high load levels until the peak. In the FEM simulation, the ETS bars are triggered at higher forces than

those observed in the experiment. The strains determined in the FEM simulations are smaller than the strains read at gauges in the experiments at whole curves. This is attributable to that the actual adhesive stiffness might accelerate the reading of strain gauges. Meanwhile, the cohesive law assumed for that ETS-GFRP bar–concrete contacts in the FE models may delay the progression of the strain in ETS bars.





Note: Gray zone shows maximum principal strain areas, where exceeded the ultimate strain.

Figure 4. Validations of FE models: (a) load versus deflection; (b) load versus strain in ETS bars; (c) maximum strain in steel stirrups, ETS bars, and longitudinal steel bars; (d) failure patterns

The collapse mechanisms of the ETS-intervened beams observed in both tests and simulations are depicted in Figures 4-c and 4-d. In the numerical analyses, at the completion of failure (i.e., last step of FEM), the steel stirrups yielded following by concrete fracture in the shear span center of beams. The ETS bars did not rupture, and the steel tensile bars did not yield. These observations are identical to the actual experiments. The real shear diagonal cracks in the test beams have taken place in the region where the maximum principal strain found by simulations exceeded its maximum strain, as displayed in Figure 4-d. Additionally, the FE analyses characterized by the maximum principal strain suitably reflected the bending and compressive deformations observed in the test beams. Further, the beam C2 illustrates a safe mode of failure, in which the sudden collapse in shear was prevented and replaced by the early-warning concrete crushing at loading region (as depicted in Figure 4-d). The beam C2, which was strengthened by the diagonal ETS bars (i.e., large percentage and long bonded length), could bring more efficient shear resisting behavior.

4. Parametric Studies by Means of FE Analyses

4.1. Introduction to Variables

Critical design parameters for the ETS-strengthened beams are the strength of concrete under compression (f'_c), the increase of total stiffness ($E_f p_f + E_{sw} \rho_{sw}$) as decreasing stiffness ratio of ETS bars to existing steel stirrups ($E_f p_f / E_{sw} \rho_{sw}$), and the section geometries and shear span over effective depth (a/d) ratios. This section considers the analyses on the structural behaviors of the ETS-strengthened beams under various design parameters. Additionally, along with the experimental data, the numerical shear capacities of the specimens achieved from the FE analyses provide a large data pool for proposals of the shear resistance model in this study as well as the other works [21]. The shear performance including the capacity, deformation, failure mechanism, reinforcement strain, and ductility are assessed. Notably, the ductility is defined by absorption energy, which is calculated by the area underneath a load–deflection plot at the peak load. The larger the absorption energy, the higher the ductility. Aside from investigating new design parameters, the outcomes of the parameteric studies are verified with the outcomes of the available experiments.

4.2. Effects of Increasing of $E_f \rho_f + E_{sw} \rho_{sw}$ as Decreasing of $E_f \rho_f / E_{sw} \rho_{sw}$ among Different f'_c

4.2.1 Load versus Deflection and Failure Characteristics

The beams in the groups G0, G1, and G2 are created to investigate effects of increasing total stiffness $(E_f \rho_f + E_{sw} \rho_{sw})$ by decreasing stiffness ratio $(E_f \rho_f / E_{sw} \rho_{sw})$ under the different concrete strengths due to compression (f'_c) , as displayed in Table 1. The concrete compressive strengths employed in the beam groups G0, G1, and G2 are 20, 38, and 70 MPa, respectively. The stiffness ratios are designed to decrease from 0.564 down to 0.160, while the total stiffness values are designed to increase from 302.4 up to 911.1 MPa.

Figures 5-a to 5-c present the load—displacement responses of the retrofitted beams among three groups of concrete compressive strength. As indicated in Figures 5-a to 5-c, the concrete cracking force is higher as the compressive strength of concrete is greater. All ETS-strengthened beams are characterized in three stages: (i) before concrete cracking, (ii) steel yielding phase, and (iii) ETS contribution. Obviously, the increase in the compressive strengths of concrete enhances the rigidity and maximum load of the ETS-intervened specimens.

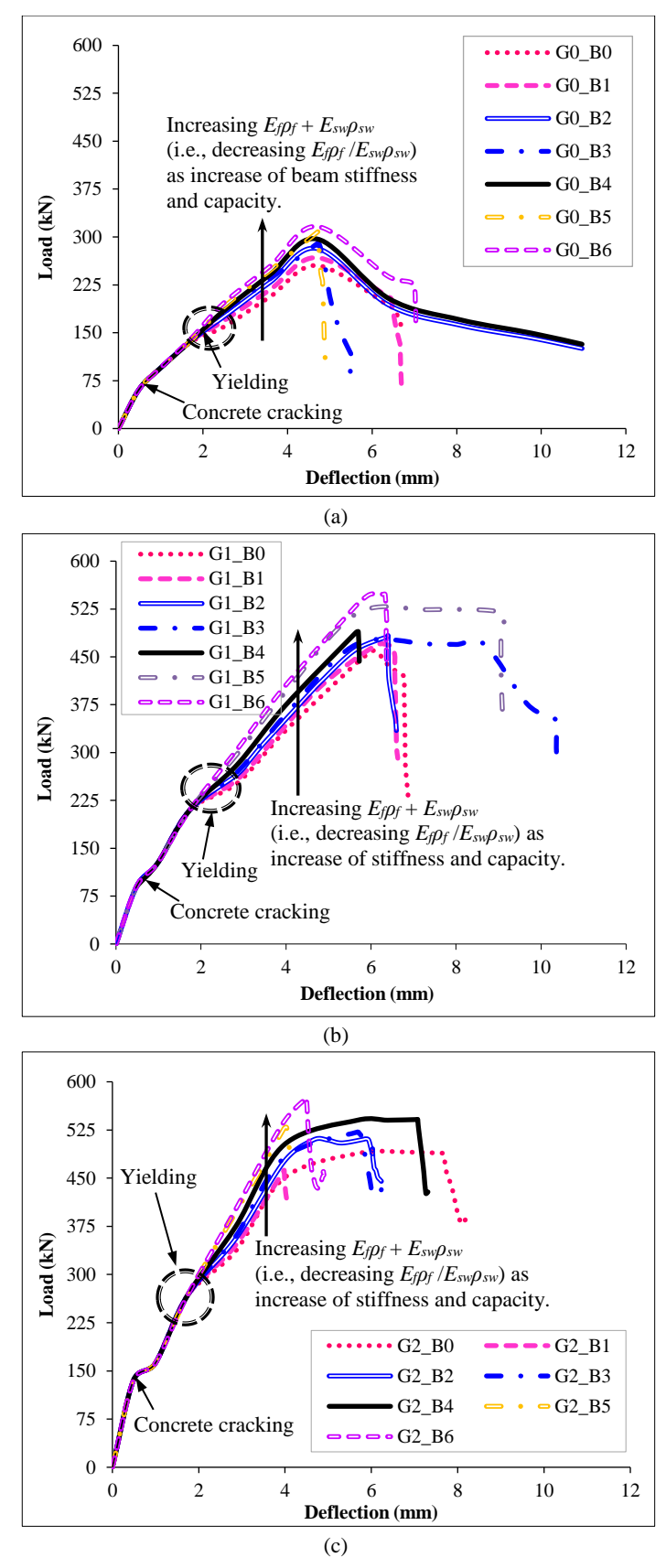
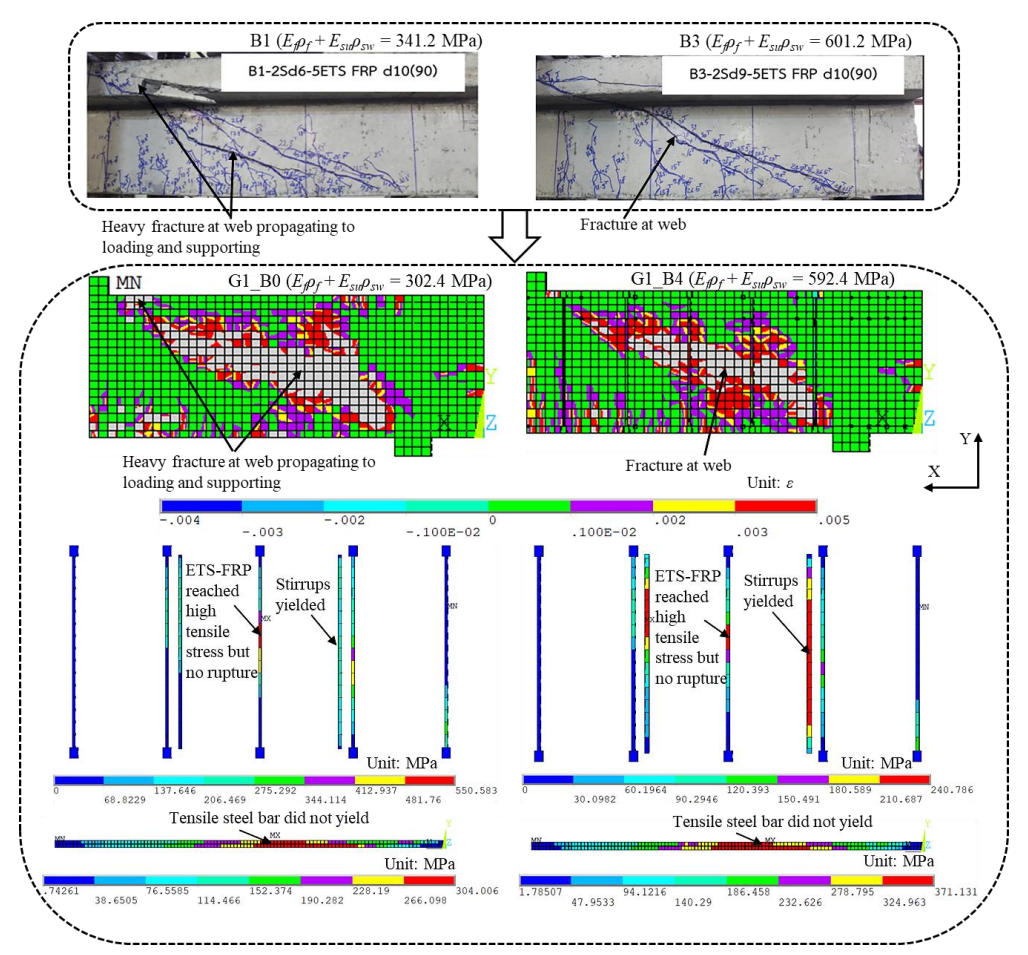


Figure 4. Load–deflection curves: (a) $f'_c = 20$ MPa; (b) $f'_c = 38$ MPa; (c) $f'_c = 70$ MPa

In case of the same f'_c , the responses of the ETS-retrofitted specimens with distinct values of the steel shear reinforcement and ETS strengthening stiffnesses prior to the yielding loads is seemingly similar. The shear reinforcement and strengthening stiffnesses substantially affect the post-yielding behavior of the ETS-strengthened beams. In Figures 5-a to 5-c, the increase of $E_f p_f + E_{sw} \rho_{sw}$ (as decrease of $E_f p_f / E_{sw} \rho_{sw}$ ratio) results in the increase in beam stiffness, yielding force, and peak load. The primary reason is that the higher the total stiffness contributed to the improvement of overall beam stiffness, leading to the greater the shear resisting behavior. The ETS-strengthened beam

with smaller $E_{IPP}/E_{sw}\rho_{sw}$ ratio increases the yielding load to be closer to the maximum load.

Figure 6 shows the failure mechanisms in the ETS-intervened specimens due to the influence of the increase in total stiffness ($E_f \rho_f + E_{sw} \rho_{sw}$) by comparison between tests and simulations. Two beams in an experimental program implemented by Bui et al. [14] are B1 ($E_f \rho_f + E_{sw} \rho_{sw} = 341.2$ MPa) and B3 ($E_f \rho_f + E_{sw} \rho_{sw} = 601.2$ MPa), while two beams in the parametric study of the present work that have similar total stiffnesses to tested beams are G0_B0 ($E_f \rho_f + E_{sw} \rho_{sw} = 302.4$ MPa) and G0_B4 ($E_f \rho_f + E_{sw} \rho_{sw} = 592.2$ MPa). The ETS-strengthened beam was heavily deteriorated with smaller total stiffness since in this situation the shear resistance mechanism was majorly responsible by the concrete. The beam with lower total stiffness induces more compressive fracture at the loading area. The FE analyses show the similar trend to the experimental monitoring via the principal strain contour. The stirrups in two cases were yielded, while no rupture in the ETS bars was recognized. The stress in ETS-FRP bars in the beam G0_B0 with $E_f \rho_f + E_{sw} \rho_{sw} = 302.4$ MPa was higher than that in the specimen G0_B4 with $E_f \rho_f + E_{sw} \rho_{sw} = 592.4$ MPa because the latter case had lower elasticity of modulus of ETS-FRP bars ($E_f = 50$ GPa). Moreover, the beam with larger $E_f \rho_f + E_{sw} \rho_{sw}$ triggered the greater stress in the longitudinal steels than that in the longitudinal reinforcing bars of the member with smaller $E_f \rho_f + E_{sw} \rho_{sw}$. No global debonding (i.e., slippage) of the ETS elements from surrounding concrete was observed in both tests and FE models.



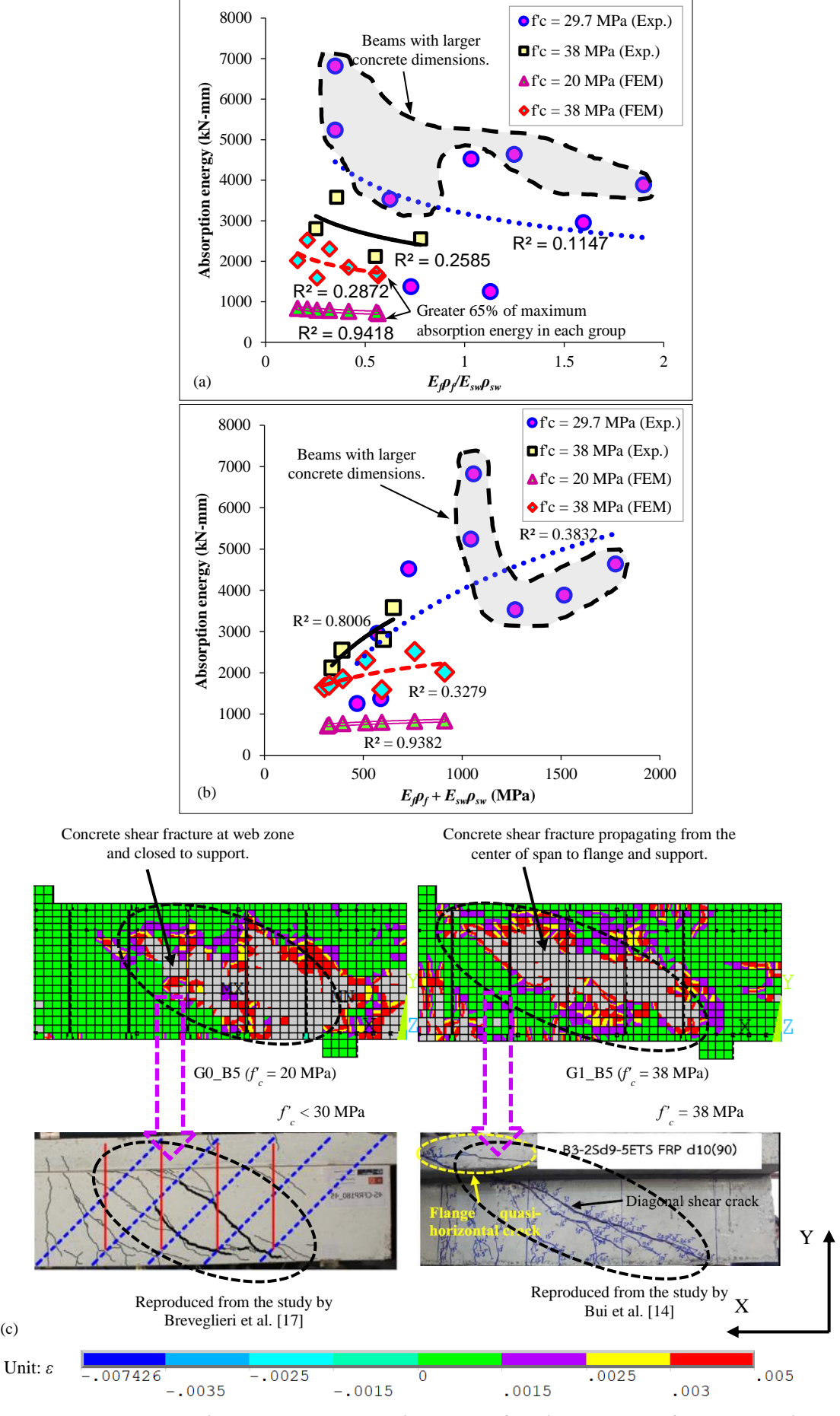
Note: Maximum principal strain in concrete exceeding ultimate strain is shown in gray color.

Figure 5. Fracture mechanism in ETS-strengthened beams with different total stiffnesses (actual crack patterns were reproduced from the study of Bui et al. [14])

4.2.2. Ductility-Based Energy

Figures 7-a and 7-b show the relationships between absorption energies of the beams and stiffness ratios ($E_f \rho_f / E_{sw} \rho_{sw}$) and total stiffness ($E_f \rho_f + E_{sw} \rho_{sw}$) for the test beams in previous studies [14–17] and the beams in the parametric studies. The purpose is to not only assess the influence of transverse steel and intervening reinforcement stiffnesses on the beams' ductility but also verify the accurateness of the FE analyses to the experiments in the ductility evaluation. As mentioned above, the ductility of the ETS-FRP-strengthened beams is determined through energy, which is calculated by the area underneath the prepeak regime of the load–deflection curve. The ductility increases as the absorption energy increases. Note that the specimen D1 is not considered in this section due to the absence of ordinary internal steel stirrups. The dimensions of the specimens in the works of Bui et al. [14] and Breveglieri et al. [17] are identical, and they are smaller than those in the work by Mofidi et al. [16]. To compare with the experimental data in the similar concrete compressive strengths, only beams in groups G0 and G1 with $f_c^2 = 20$ and 38 MPa of the parametric studies are considered for the ductility evaluation.

(c)



Note: In FEM simulations, maximum principal strain exceeding ultimate strain is shown in gray color

Figure 7. Effects of f'_c on absorption energy: (a) $E_f \rho_f / E_{sw} \rho_{sw}$; (b) $E_f \rho_f + E_{sw} \rho_{sw}$; (c) deformation

Figures 7-a and 7-b show that the increase of $E_{f}\rho_{f}/E_{sw}\rho_{sw}$ ratios as decreasing $E_{f}\rho_{f}+E_{sw}\rho_{sw}$ reduces the absorption energies of the ETS-intervened specimens, decreasing the member ductility. The same trend is also identified by the test results. The absorption energy of the ETS-strengthened beam can correlate to the stiffness ratio or total stiffness via power or logarithmic functions with R^2 indicated in Figures 7-a and 7-b. The larger $E_f \rho_f / E_{sw} \rho_{sw}$ ratio (i.e., smaller $E_f \rho_f +$ $E_{sw}\rho_{sw}$) is, the smaller member stiffness is, inducing lesser capacity and absorption energy. Further, the beam with the greater $E_f \rho_f / E_{sw} \rho_{sw}$ ratio (i.e., smaller $E_f \rho_f + E_{sw} \rho_{sw}$) would show the earlier yielding load to abdicate from the beam capability at high load levels. For the beams having the same dimensions, the ductility-based energy increases as the enhancement of the strength of concrete in compression. The beams with larger geometry provide the greater absorption energies (i.e., larger ductily) than the beams with smaller geometry. These observations are attributable to the dependency of concrete compressive strength and beam geometry on the shear resisting efficiency of the ETSstrengthened RC beams. For beams with the same specifications as those used in the parametric studies (details provided in Table 1 and Figure 1), an $E_{t}\rho f/E_{sw}\rho_{sw}$ ratio below 0.5 can be considered for the design practice of ETS-strengthened RC specimens. This ratio was shown in the FE simulations to retain at least 65% of the maximum ductility, as indicated by the energy dissipation results in Figure 7-a. From a practical standpoint, using a lower ETS reinforcement stiffness relative to the transverse steel can help reduce the risk of reinforcement congestion, particularly in sections with limited dimensions. However, proper detailing to meet minimum spacing requirements for both ETS bars and existing steel stirrups needs further experimental investigation.

Figure 7-c demonstrates the deformation in shear zone of the ETS-strengthened beams with $f'_c < 30$ MPa and $f'_c = 38$ MPa by comparing simulation with test. Overall, the ETS-strengthened beams were with shear failure owing to the wide and opening deformation causing the fracture in concrete. This reveals in the FEM simulations by the large portion of maximum principal strains, where the actual shear cracks have taken place. In the specimen with $f'_c < 30$ MPa, the concrete principal strain heavily occurred near the support, as obtained from both experiment and simulation results. Conversely, for the beam with higher concrete compressive strength ($f'_c = 38$ MPa), the large principal strain zones at the final step of FEM modeling are intersected with the entire strengthening system and propagated to both loading and support areas. Moreover, the deformation at the soffit of the beam is pronounced in the beam with greater f'_c . Thereby, the ETS-strengthened beam with higher f'_c can delay the shear fracture of concrete aiming to efficiently trigger the shear resisting capability of steel stirrups, ETS-FRP bars, and their bond performance to concrete, leading to the more ductile failure. These mentioned phenomena agreed with the experimental behaviors well. The condition of $f'_c = 38$ MPa should be concerned in the design practice of ETS-intervened RC members.

4.3. Effect of Beam Geometry

Effects of beam geometry and a/d ratio are examined in this section. First, in Section 4.3.1, the geometrical effect on the differences of the shapes and sizes of the beam section having the same value of the shear span over effective depth ratio (a/d) is considered. Second, in Section 4.3.2, the effect of the beam having the different a/d ratios but the same shapes and dimensions is investigated.

4.3.1. Comparison between Beams with Rectangular Section and with T-Shaped Section

This section comprises three beams with different geometries: T-shaped section, large rectangular, and small rectangular. One T-shaped section beam named B_T (web: $180 \times 300 \text{ mm}^2$, flange: $450 \times 100 \text{ mm}^2$) is prepared. One large rectangular beam named B_LRec. ($180 \times 400 \text{ mm}^2$) with the same overall height and web width with the T-shaped section beam is designed. One small rectangular beam named B_SRec. ($150 \times 300 \text{ mm}^2$) with smaller section dimensions than those of the aforementioned large rectangular beam is created. All T-shaped section and rectangular beams in this section have the same concrete properties, steel reinforcing, and ETS strengthening characteristics. The shear span over effective depth ratio (a/d) of all beams investigated is 2.4. The details and specifications of the beams are illustrated in Table 2 and Figure 8. The beams are designed failing in shear at the span with ETS bars. The stirrups in the control span and the longitudinal tension bars are aimed with over-reinforced design.

Beam shape Beam ID *h* (mm) d (mm) b_w (mm) L (mm) a (mm) a/d $E_f(GPa)$ ρ_t (%) ρ_{sw} (%) ρ_f (%) f'_c (MPa) B_T 375 2.4 5.24 0.11 0.34 T-section 400 180 2450 900 50 38 Large rectangular B LRec. 400 375 180 2450 900 2.4 50 5.24 0.11 0.34 38 section Small rectangular B_SRec. 300 250 150 1950 600 2.4 50 5.24 0.11 0.34 38 section

Table 2. Beam configurations for beam geometry effects

Notes: h refers to the height of the beam section (mm); d denotes the effective depth of beam section (mm); b_w is the beam width (mm); L is the length of beam (supporting to supporting) (mm); a refers to the shear span size of the beam (mm); ρ_{sw} denotes the ratio of steel stirrups (%); ρ_t is the ratio of tensile steel bars (%); E_f is the modulus of elasticity of ETS bars (GPa); ρ_t refers to the amount of ETS bars (%); f_c denotes the compressive strength of concrete due to compression (MPa).

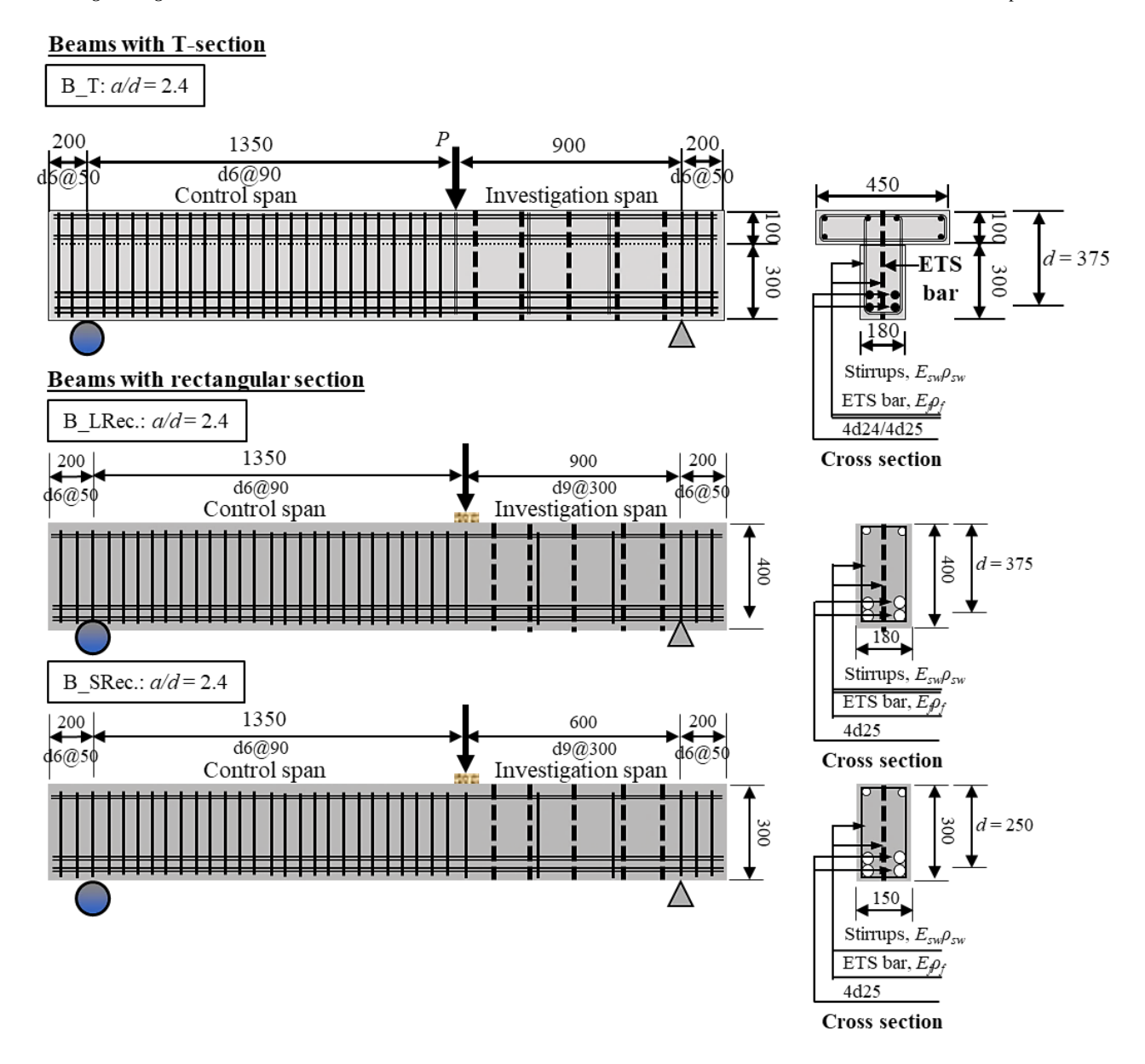


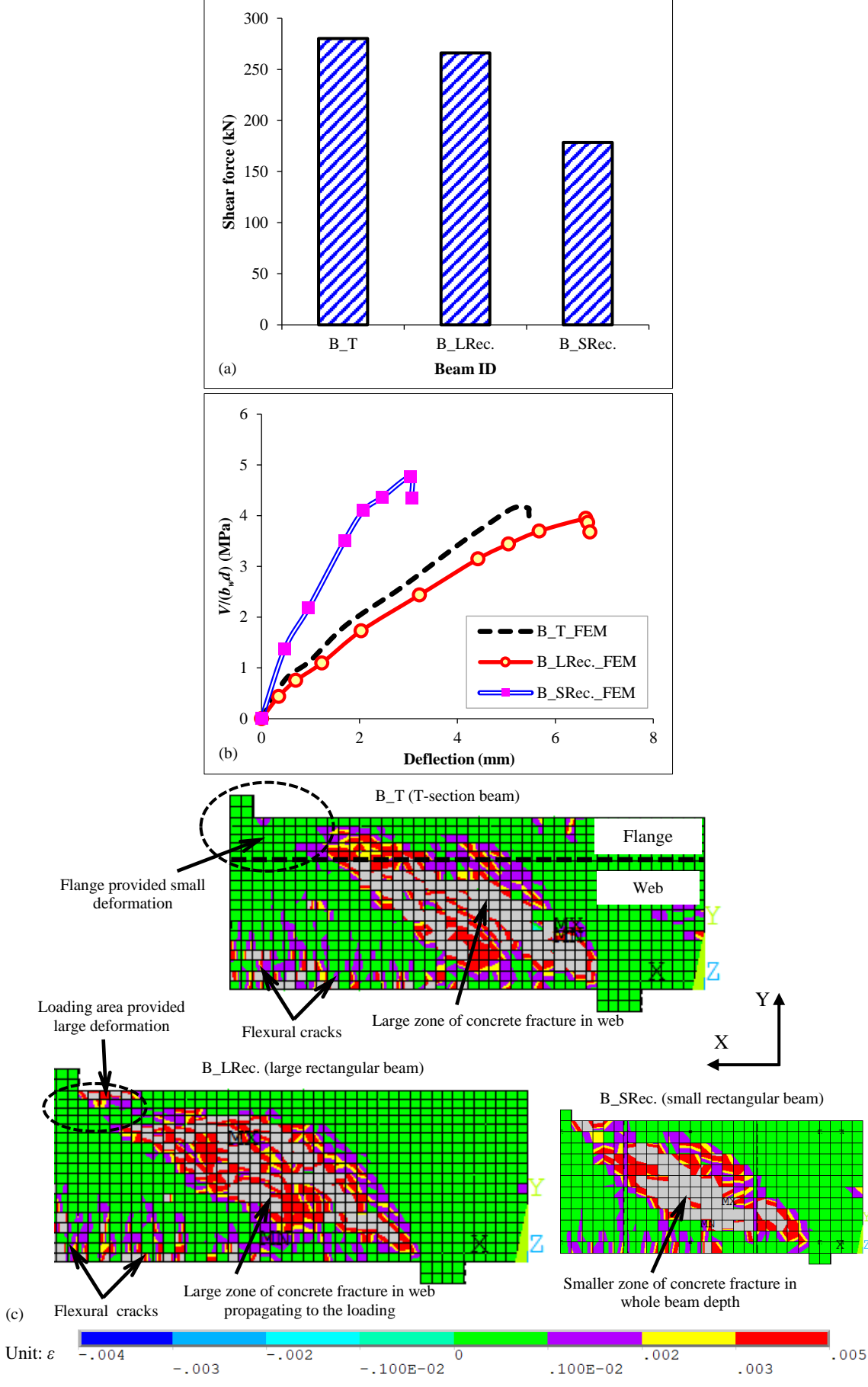
Figure 6. Beam configurations for investigation of beam geometry effects (dimensions in mm)

The nominal transverse stress of the ETS-intervened specimens can be calculated as follows:

$$v = \frac{v}{b_{w}d} \tag{5}$$

where V denotes the nominal shear strength (kN); b_w refers to the width of the beam section web (mm); d represents the section effective depth (mm).

Figure 9-a illustrates the comparison of maximum shear forces among three beam section types. Due to their larger dimensions, the T-shaped ETS-strengthened beam (B_T) and the large rectangular beam (B_LRec.) exhibit significantly higher shear capacities, approximately 57% and 49% greater, respectively, than the small rectangular ETS-strengthened beam (B_SRec.). The increased section size allows for longer ETS-FRP bar embedment and stronger chord connections, which enhance bond efficiency and enable full development of the truss mechanism. Interestingly, even with identical beam widths and overall heights, the T-section beam achieved a shear capacity about 5% higher than the large rectangular section. This suggests that while the top flange of the T-section may contribute marginally, its effect on shear strength within the ETS system is relatively limited. These results emphasize the impact of geometric configuration on the performance in shear of ETS-retrofitted members. Similar observations on geometrical effects have been reported in previous studies involving externally wrapped FRP sheets by Leung et al. [32] and Benzeguir et al. [33].



Note: Maximum principal strain exceeding ultimate strain is displayed with gray color.

Figure 9. Investigations of geometrical effects: (a) shear-bearing capacity; (b) nominal shear stress versus deflection; (c) principal strain distribution in concrete

Figure 9-b presents nominal shear stress (v)—deflection curves, offering further insight into the impact of beam geometry. Notably, the small rectangular beam exhibits higher nominal shear stress than both the T-section and large rectangular beams. This is primarily attributed to the increasing shear-resisting area ($b_w d$) in larger sections, which diminishes the stress. Between the T-section and large rectangular beams, both having the same width and height, the T-section demonstrates greater stiffness, likely owing to the resisting contribution of the critical loading zone of the flange. Moreover, the small rectangular beam, owing to its shorter span, also shows superior stiffness. In this case, a significant amount of the load is carried by the arching action in concrete, while the ETS rods effectively limit vertical displacement. In other words, for a constant a/d ratio, shallower beams may perform better in terms of shear stress and stiffness—primarily due to enhanced concrete action—compared to deeper beams. This size-related effect is consistent with the observations documented in ACI 318-19 [24].

Figure 9-c shows the principal strain distribution in the shear span regions of the three specimens at the final step of the FE analysis. It highlights that the region of high principal strain increases with beam size. This is because the T-shaped and large rectangular beams, with wider shear spans, allow greater bridging action of ETS bars and stirrups across diagonal cracks. These beams also offer longer embedment lengths for the ETS bars, which facilitate more effective stress transfer and distribution along the bonded interface. The flange of the T-shaped beam helps reduce deformation at the loading area by contributing to the compression zone. Similar observations were reported by Benzeguir et al. [34] in EB-FRP-wrapped beams, where larger specimens exhibited wider shear cracks due to early degradation of aggregate interlock. Future studies should consider concrete constitutive models that account for aggregate interlocking effects to better capture the influence of beam geometry in ETS-strengthened systems.

4.3.2. Change of a/d Ratios

The rectangular beams B1_a/d1.6, B2_a/d2.4, B3_a/d3.6, and B4_a/d4.8 presented in Table 3 and Figure 10 are used to extend a parametric study on the change of the values of the shear span length over effective depth ratio (a/d). These beams are designed to have the same concrete section and properties, ETS strengthening bars, and steel reinforcement, but different a/d values. The a/d ratios for the members B1_a/d1.6, B2_a/d2.4, B3_a/d3.6, and B4_a/d4.8 are 1.6, 2.4, 3.6, and 4.8, respectively.

Beam shape	Beam ID	h (mm)	d (mm)	b _w (mm)	L (mm)	a (mm)	a/d	$E_f(GPa)$	ρ _t (%)	ρ _{sw} (%)	ρ _f (%)	f'c (MPa)
Rectangular section	B1_a/d1.6	300	250	150	800	600	1.6	50	5.24	0.11	0.34	38
	B2_a/d2.4	300	250	150	1200	600	2.4	50	5.24	0.11	0.34	38
	B3_a/d3.6	300	250	150	1800	900	3.6	50	5.24	0.11	0.34	38
	B4_a/d4.8	300	250	150	2400	1200	4.8	50	5.24	0.11	0.34	38

Table 3. Specifications of beams for parametric studies on geometry and a/d ratio

Notes: h refers to the height of the beam section (mm); d denotes the effective depth of beam section (mm); b_w refers to the beam section width (mm); L is the length of beam (supporting) (mm); a means the length of the shear span of the beam (mm); ρ_{sw} refers to the amount of steel stirrups (%); ρ_s is the ratio of tensile steel bars (%); f_s is the modulus of elasticity of ETS rods (GPa); ρ_s denotes the percentage of ETS bars (%); f_s refers to the concrete compressive strength (MPa)

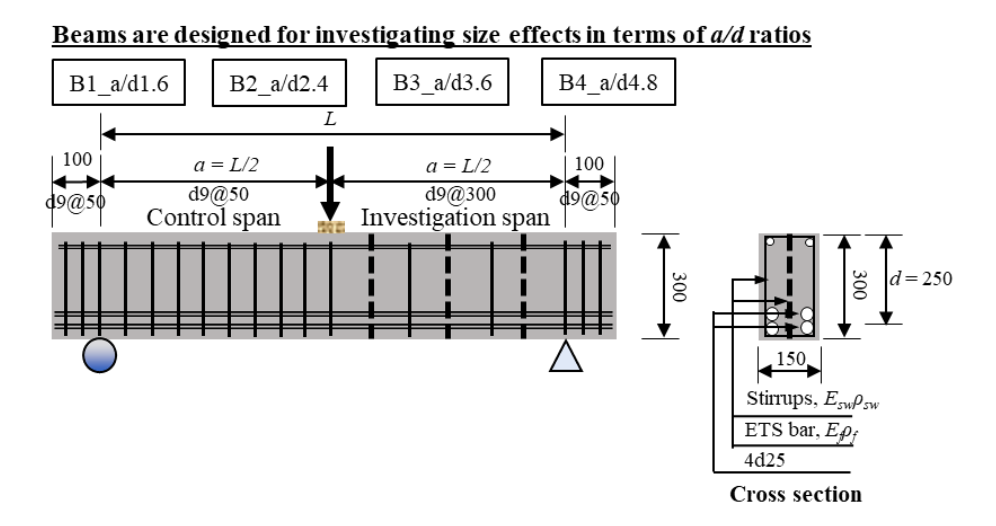


Figure 7. Beam configurations for investigation of a/d ratios (dimensions in mm)

Figure 11 demonstrates the load–displacement relationships for four beams with different a/d values. Obviously, the stiffness and maximum shear force of the ETS-intervened specimens decreased with increasing of a/d values. The maximum capacities of the beams B1_a/d1.6 (a/d = 1.6), B2_a/d2.4 (a/d = 2.4), B3_a/d3.6 (a/d = 3.6), and B4_a/d4.8 (a/d = 4.8) are 438, 357, 270, and 190 kN, respectively, while their deflections at peak loads are 1.62, 3.03, 6.59, and 8.65 mm, respectively. Figure 11 also reveals the presence of the yielding of existing stirrups before peak load in the specimens with a/d = 2.4 and 3.6, while no yielding of stirrups prior to peak load for the specimens with a/d = 1.6 and 4.8 was observed. This result is attributable to that the concrete arch action in the specimen with a/d = 1.6 and the flexural mechanism in the beam with a/d = 4.8 delay the yielding of shear transverse steel.

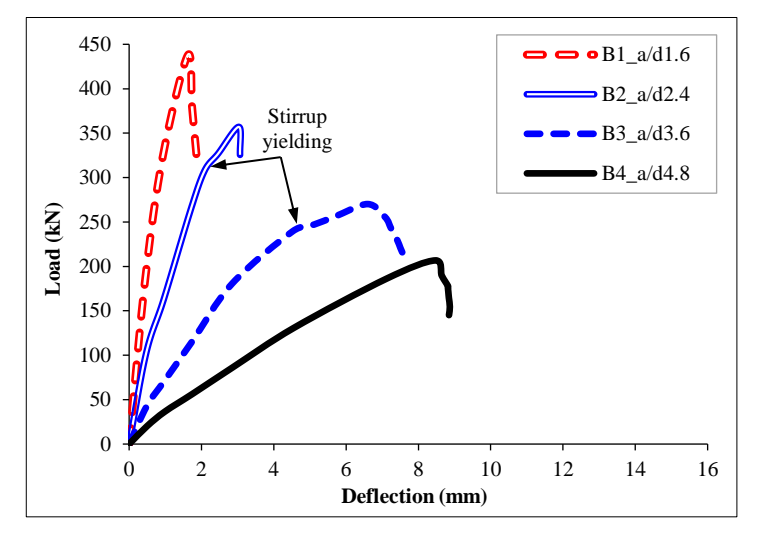
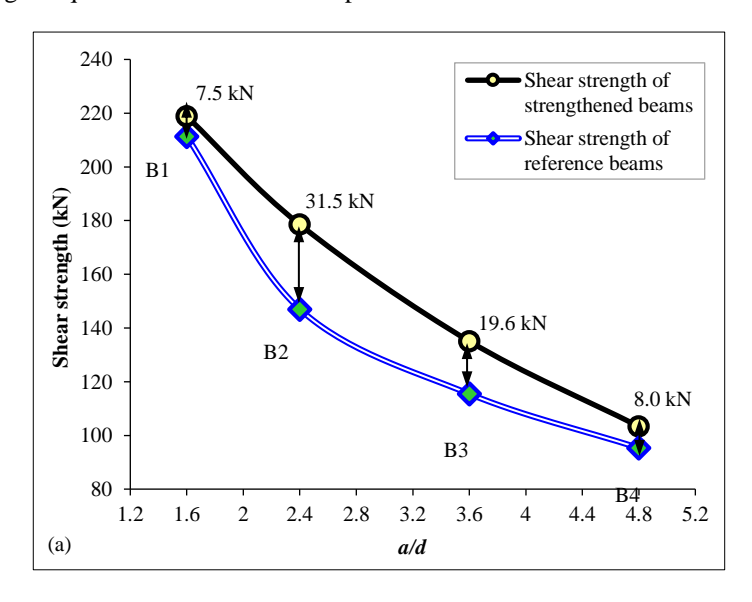


Figure 8. Effects of a/d ratios on load-deflection relationship

Figure 12-a demonstrates that the ETS shear resisting force decreased as the increase of a/d ratios from 2.4 up to 4.8, while it increased as the increase of a/d ratios from 1.6 up to 2.4. Notably, the ETS shear contribution is defined by the discrepancy in the peak shear load between the control beam (no ETS) and the intervened specimen (with ETS). Conversely, Figure 12-b presents the maximum deformation in ETS rods distributed along the maximum principal region from the loading to the supporting. The strain in the ETS intervening elements disperses in different manners among the beams with different a/d ratios.

The major causes for the above-mentioned results are shown in the explanations as follows. The ETS-strengthened beams with different a/d ratios would demonstrate different failure mechanisms, as displayed in Figure 13. This leads to that the shear resisting mechanisms of deep embedment retrofitting system in those specimens are distinct. For instance, for the beam with a/d = 1.6, the concrete arch mostly takes responsible for the shear applied loads. Hence, the ETS intervening elements in that beam are not effectively utilized, and that beam behaves stiffener and inductile. For the specimen with a/d = 2.4, along with truss action, the concrete arch partially undertakes in resisting the shear transfer forces. The ETS-FRP strengthening bars could play both roles (i) bridging to restrict the vertical deformation of the beam, and (ii) truss chords to carry the shear stress. Thereby, the ETS shear contribution can be efficiently triggered. In Figure 13, for the beams with a/d no greater than 2.4, no clear difference in the maximum principal strain between peak load and failure completion was observed. This means that the beam with low a/d ratio shows a formation of concrete strut at peak load, causing the quick load reduction after peak.



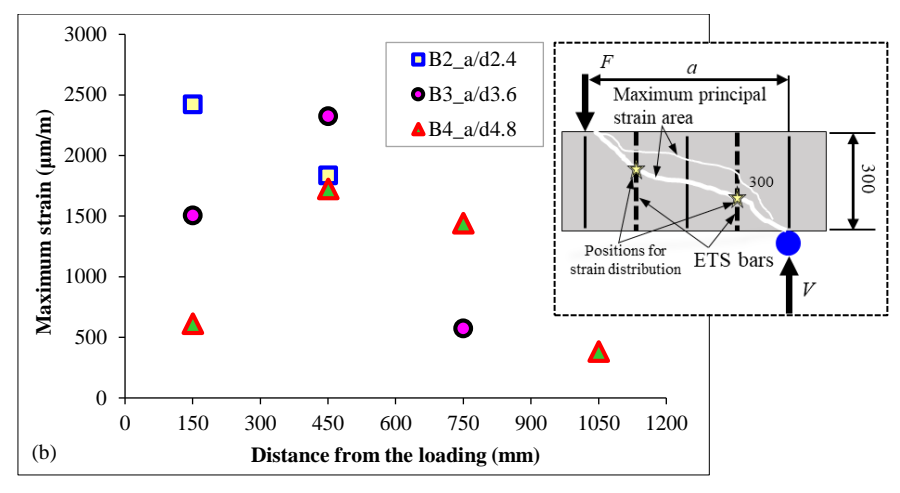


Figure 9. Effects of a/d values: (a) shear strength; (b) strain distribution in ETS bar along maximal principal strain

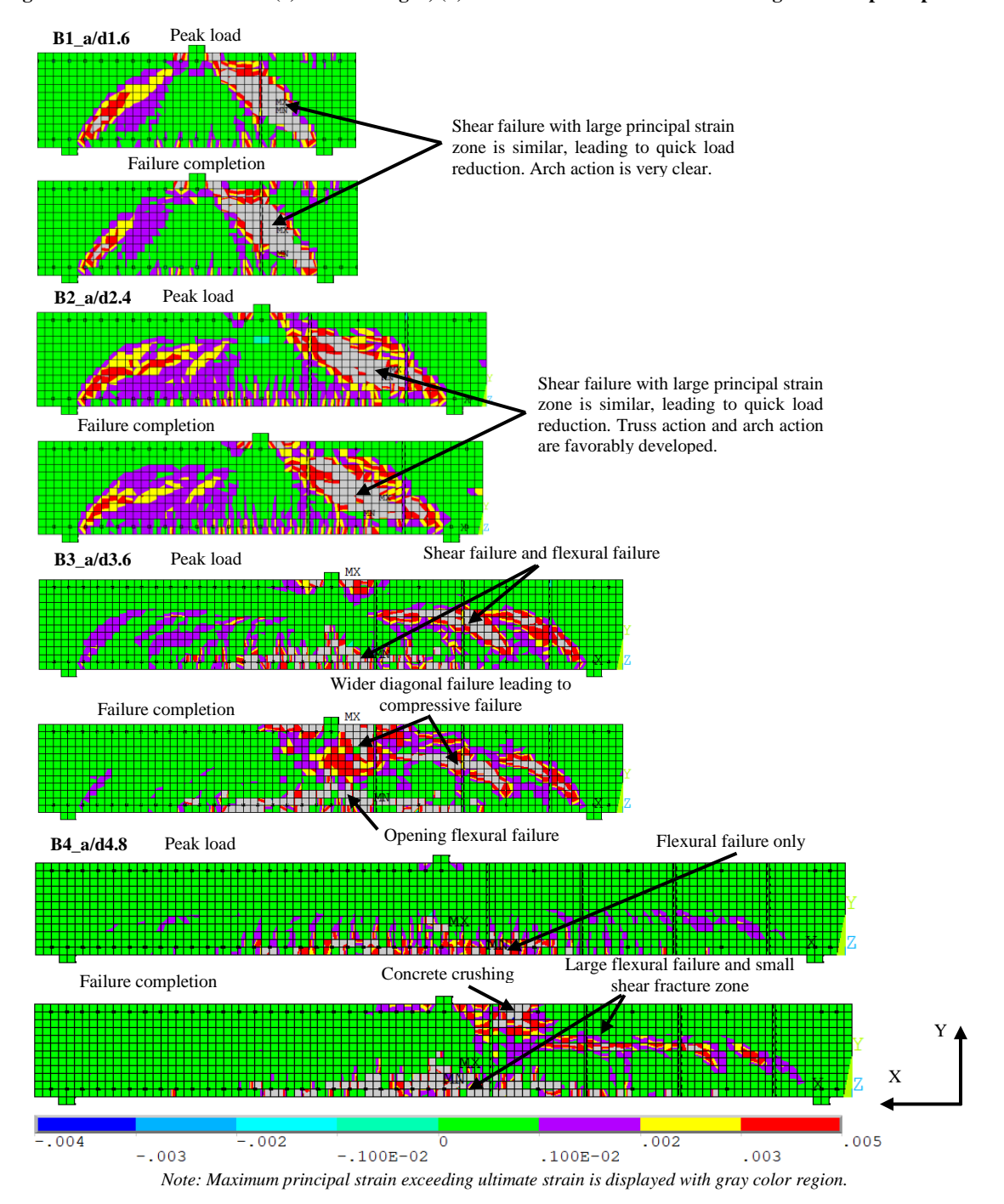


Figure 10. Effects of a/d ratios on failure mechanism

When increasing a/d ratios up to 3.6 and 4.8, the arch action in the beam becomes small or even negligible. Figure 13 illustrates that there are strain developments in the principal compressive and diagonal strains in the beams with a/d = 3.6 and 4.8 from the peak force to the completed failure, indicating the slow load reduction after peak. The beam with a/d = 3.6 would fail in the flexural crack opening following by the diagonal-compressive fracture (as indicated in Figure 13). Meanwhile, the beam with a/d = 4.8 mainly behaves as a flexural member, in which the longitudinal reinforcement was more activated, and the beam fractured by crushing of concrete at loading after the wide flexural cracks (as indicated in Figure 13). In this situation, the shear fracture zone was small, hence the efficiency of ETS-FRP retrofitting rods in resisting the shear was not high. In conclusion, the ETS strengthening system in the beam with a/d = 2.4 is most effective. All phenomena and findings achieved in this section agreed well with the literature by Leung et al. [33], Benzeguir et al. [34], and Li & Leung [35] regarding the EB-FRP strengthening technique.

5. Evaluation of Shear Strength Models

This section assesses the accuracy of the shear resisting equations furnished in the guidelines of ACI 440.1R-15 [24] and JSCE [25] for estimation of the maximum shear strength of ETS-intervened beams and the contribution in shear of ETS-retroftting elements. The model verifications are made using the data from the tests and the parametric studies for the ETS-strengthened beams shown in Table 1. The influences of the concrete strength in compression, stiffness of ordinary internal steel stirrups, and stiffness of ETS-FRP intervening are included in the assessment of the shear resisting models.

The total shear force of a RC beam retrofitted with ETS rods can be derived as follows:

$$V_n = V_c + V_s + V_f \tag{6}$$

where V_n refers to the total beam shear capacity (kN); V_c denotes the shear load provided by concrete (kN); V_s denotes the shear resisting force carried by stirrups (kN); V_f refers to the shear resistance of ETS intervening rods (kN).

The models of the resisting force in shear of concrete (V_c) in the ACI 318 [23] and the JSCE [25] codes stipulate the following expressions:

$$V_c = 0.29\sqrt{f_c'}b_w d \tag{7-a}$$

$$V_c = 0.2\sqrt[3]{f_c} \sqrt[4]{\frac{1000}{d}} \sqrt[3]{100\rho_w} b_w d$$
 (7-b)

where f'_c refers to the concrete strength due to compression (MPa); b_w denotes the width of the beam section web (mm); d means the section effective depth (mm). In Equation 7-a, as suggested by Breveglieri et al. [13], the coefficient 0.29 is obtained from the mean of the interval of concrete shear capacity offered in the ACI 318 [23].

In the ACI 318 [23] and the JSCE [25] guidelines, the shear load of internal transverse steel can be derived applying the truss analogy as below:

$$V_{S} = A_{v} f_{y} \frac{d(\cot \theta + \cot \alpha)}{S} \sin \alpha$$
 (8-a)

$$V_{s} = A_{v} f_{y} \frac{7d(\cot \theta + \cot \alpha)}{8s} \sin \alpha$$
 (8-b)

where f_y denotes the yielding stress level of steel reinforcing bars (MPa); s refers to the ordinary stirrup spacing (mm); d refers to the effective depth (mm); A_v denotes the cross-section area of internal steel reinforcement (mm²); α and θ refer to the reinforcement inclination and shear diagonal crack angle (°). The shear diagonal crack inclination (θ) is simply assumed by 45°.

The shear contribution of ETS strengthening bars uses the following equation:

$$V_f = A_f E_f \varepsilon_{fe} \frac{d(\cot \theta + \cot \alpha)}{s} \sin \alpha \tag{9}$$

where ε_{fe} is the effective strain of ETS strengthening system (μ m/m); A_f refers to the cross-section area of ETS intervening rods (mm²); E_f denotes the elastic modulus of ETS retrofitting bars (GPa); for ETS bars, the section effective depth d is taken as the specimen section height h (mm).

The effective strain equations ε_{fe} for FRP shear intervening system proposed in the ACI 440.1R-15 [24] and JSCE [25] standards are respectively depicted as below:

$$\varepsilon_{fe} = min\left(0.004, \varepsilon_{f,u}, \frac{0.05r_b}{d_f} + 0.3\right) \tag{10-a}$$

$$\varepsilon_{fe} = \sqrt{\left(\frac{\Box}{0.3}\right)^{-0.1} \times f_c' \times \frac{\rho_s E_s}{\rho_f E_f}} \times 10^{-4} \tag{10-b}$$

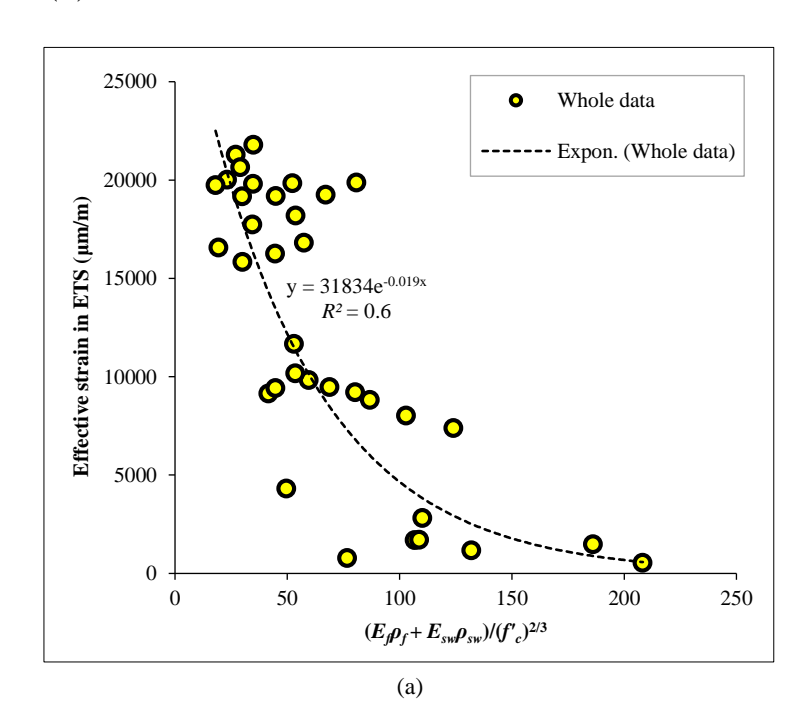
where $\varepsilon_{f,u}$ refers to the ultimate strain of ETS bars (µm/m); r_b is the bent radius of the ETS intervening rods (mm); d_f denotes the ETS bar diameter (mm); h refers to the section height of the beam (mm); E_f denotes the modulus of elasticity of the ETS retrofitting rods (GPa); ρ_f refers to the percentage ratio of ETS intervening elements (%); E_s denotes the modulus of elasticity of the tensile steel reinforcement (GPa); ρ_s represents the ratio amount of the flexural steel reinforcement (%).

Several previous studies, for an example Bui et al. [14], concluded that the results made by shear strength models for ETS-FRP contribution in the above-mentioned guidelines underestimated the experimental ETS-FRP shear contribution, especially the beams with ETS-GFRP bars. The main reasons are caused by the following argumentations. The ETS-FRP intervening bars are inserted through whole section, particularly the cases with inclined arrangement or with anchorage, for ensuring that the actual truss mechanism can be fully acted. Additionally, the ETS-FRP bars are surrounded by concrete for providing an efficient confinement action to prevent the premature deterioration due to the shear applied forces acted to concrete arch. On the other words, the ETS strengthening bars can play two roles: (i) the tension chords undertake the high tensile capacity, and (ii) join with concrete arch to resisting the shear compressive force transfer.

Aside from the well-known works by Triantafillou et al. [36], Breveglieri et al. [18], and Bui et al. [14], the FE analyses in Section 4.2 indicated that the performance of FRP shear strengthening system bonded to the concrete substrate in the shear region of the members depended on the FRP stiffness, existing stirrup stiffness (if applicable), and concrete strength under compression. One of the physical meanings of that dependency is that the increase of compressive strengths of concrete obviously improved the member capacity and stiffness of the ETS-retrofitted specimens, increasing the strain in ETS strengthening bars. Another physical meaning is rather obvious that the increase in the rigidity of the shear reinforcement and strengthening elements diminished the deformation in ETS strengthening system. The effective strain formulations for ETS intervening elements in previous works were proposed without using wide design parameters and their data. Therefore, large data base and results attained from the experimental studies [14-17] and the parametric studies in Section 4.2 are used to propose a new equation for computing the effective strain in ETS retrofitting rods. Initially, the empirical and numerical effective strain for ETS retrofit can be derived as Equation 11-a. Then, the correlation between the term $(E_{\parallel}p_f + E_{sw}p_{sw})/(f^2c)^{2/3}$ and ETS effective strain is made as Figure 14-a. With $R^2 = 0.6$, the best fitting equation demonstrated the correlation can be written by Equation 11-b. Notably, this model assumes that there is no global debonding failure between ETS strengthening bars and concrete, which was observed from tests and simulations.

$$\varepsilon_{fe} = V_{f(FEM/exp.)} / \left[A_f E_f \frac{d(\cot \theta + \cot \alpha)}{s} \sin \alpha \right]$$
 (11-a)

$$\epsilon_{c} = 31834e^{-0.019 \times \frac{E_f \rho_f + E_{SW} \rho_{SW}}{\left(f_c'\right)^{2/3}}}$$
(11-b)



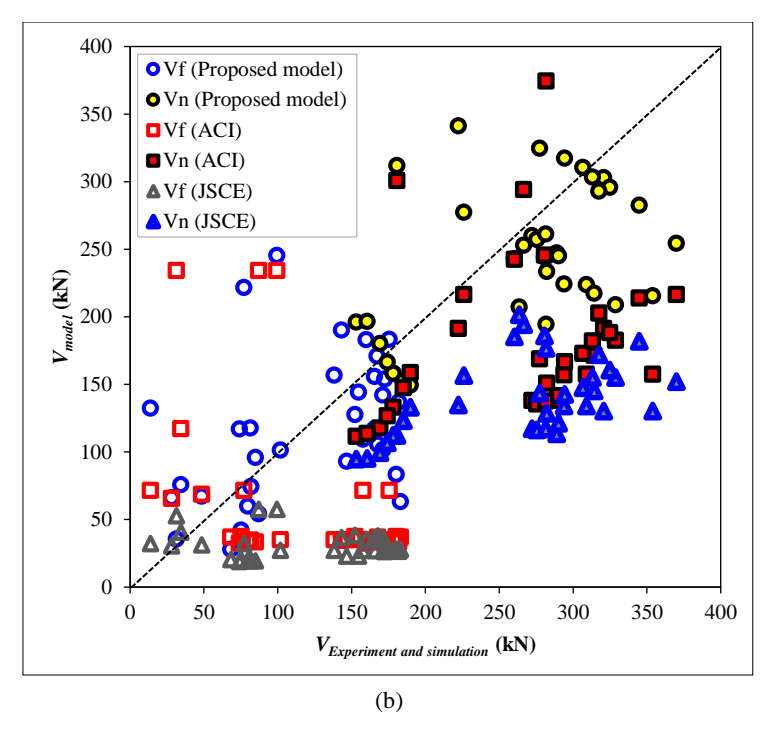


Figure 14. Validation of shear strength models: (a) proposition of ETS effective strain equation; (b) comparison

Figure 14-b demonstrates the comparison in the ETS shear contribution (V_f) and the maximum shear strength of ETS-strengthened beam (V_n) between the models, experiments, and FE analyses. The proposed model uses the equations for shear strengths of concrete and steel stirrups in the ACI 318 [23], while the proposed expression for ETS effective strain in Equation 11-b is utilized for estimation of the contribution of ETS intervening bars. The statistical values for the means of the ratios of the calculation values to the results obtained from the FEM simulations or experiments, and the coefficients of variation (C.O.V.) of the means are presented in Table 4. The results illustrate that the shear resisting force of the ETS retrofitting bars and the shear capacity of the ETS-intervened beams reproduced by the JSCE model [25] under-designed their shear capacities made by the experiment and FEM simulation. The couples of the mean and coefficient of variation are (0.40, 117%) and (0.51, 21%) for the ETS shear contribution and the maximum shear strength of the intervened beams, respectively. The primary reason is attributable to the conservativeness of the shear strength models for existing transverse steel and FRP bars in the JSCE guideline [25]. Nevertheless, the calculations constituted by the shear resisting models in the ACI guidelines [23, 24] for components of ETS-strengthened beams could improve the predictability. Despite the shear strength models provided by the ACI guidelines [23, 24] are under-designed, the mean values gained from the results estimated by the ACI guidelines [23, 24] get closer to 1.0.

Conversely, the proposed model could give an excellent prediction for the nominal shear capacity of the ETSretrofitted beams via the mean and C.O.V. equalled to 0.94 and 25%, respectively. However, the diagnosis of the shear contribution of the retrofitting bars in the intervened specimens identified by the developed model overdesigned the ETS shear resisting forces provided by the simulations and experiments. The main cause is the data dispersion of the effective strain predicted by Equation 11-b. Generally, there is a significant scatter in the prediction results for the ETS shear strength for all three models. It is observed from the measured results in the experiment by Breveglieri et al. [17] that the beam C3 (originally named 4S-C180-90 in their study) has failed with very low shear contribution of ETS-CFRP strengthening bars. Such result might be due to the early loss of adhesion of CFRP to concrete or the large number of steel stirrups, decreasing the carrying force in shear of the ETS-CFRP retrofitting system. Therefore, the ignorance of the data of the beam C3 from all calculations is examined. The recalculations for the maximum shear forces of ETS bars and ETS-intervened beams are then made. The results identify that the proposed model is the reasonable choice for approximations of both ETS and beam shear strengths, as evident in Table 4. Although the developed model for prediction of the ETS shear resistance remains less conservative, the over-design with the mean by 1.08 can be acceptable in some circumstances. Meanwhile, the proposed model furnishes safety and optimality for estimation of the shear capacity of ETS-intervened specimens with the average by 0.93. Particularly, the deviation of the estimation for the ETS shear contribution made by the proposed model is significantly reduced after ignoring unsuitable data. Therefore, the model developed in this study is more rational and reliable than the other existing models.

Table 4. Accuracy of models

Statistical analysis	Propose	ed model	ACI mod	lel [23, 24]	JSCE model [25]					
Statistical analysis	V_{f_pred} ./ $V_{f_FEM/exp}$.	V_{n_pred} / $V_{n_FEM/exp}$.	V_{f_pred} / $V_{f_FEM/exp}$.	$V_{n_pred.}/V_{n_FEM/exp.}$	V_{f_pred} / $V_{f_FEM/exp}$.	$V_{n_pred.}/V_{n_FEM/exp.}$				
Before ignoring the large scatter values for beam C3										
Mean	1.32	0.94	0.96	0.73	0.40	0.54				
C.O.V.	1.17 0.25		1.64 0.40		1.17	0.21				
		After ignoring	the large scatter value	es for beam C3						
Mean	1.08	0.93	0.84	0.72	0.35	0.54				
C.O.V.	0.56 0.26		1.70 0.41		0.99	0.21				

6. Conclusions

The outcomes of the finite element–based parametric investigations reveal novel insights into the shear response of concrete beams retrofitted with ETS bars. The key conclusions are summarized below:

- The FEM simulation is a reliable and simple tool to analyze the shear mechanism of concrete beams intervened with ETS-FRP rods. The increase of compressive strength of concrete (f'c) resulted in the enhancement of the performance of the ETS-retrofitted specimens in terms of the load-bearing capacity and stiffness. Additionally, the increase of the total stiffness ($E_{sw}\rho_{sw} + E_{f}\rho_{f}$) by decreasing the stiffness ratio ($E_{f}\rho_{f}/E_{sw}\rho_{sw}$) ameliorated the member capacity, rigidity, and ductility-based energy of the ETS-retrofitted RC beams. Owing to the benefit in the shear performance, the configurations of ETS-strengthened beams with $E_{f}\rho_{f}/E_{sw}\rho_{sw}$ ratio less than 0.5 and f'c approximated by 38 MPa should be considered for the practical application of the ETS strengthening technique.
- The presence of a geometrical effect in terms of shape section on the shear response of the intervened specimens when using the ETS-FRP strengthening scheme was found. The nominal stress in shear of the small rectangular beam was generally greater than those of the T-section and large rectangular beams. Meanwhile, the larger section beams provided the greater shear-bearing capacity. The shallower beam was deemed to be more beneficial in the specimen stiffness and shear strength than the deeper beam. Conversely, the fracture failure deformation would be increased with the beam size, while the flange of T-section beam could restrict the deformation development at the loading area.
- The increase of the a/d ratios decreased the rigidity and peak capacity of the ETS-intervened beams. The ETS-strengthened beams with a/d = 1.6 exhibited a quick load drop after the peak due to the heavy compressive failure in concrete arch. The members with higher a/d values provided a more ductile fracture due to the formations of shear truss action and flexural behavior. The deformation in ETS rods along the diagonal principal failure strain distributed in different manners. Conversely, when a/d ratios were less than 2.4, the contribution in shear of ETS intervening elements increased as the a/d ratios increased. Inversely, the ETS shear strength decreased as the a/d ratios increased when a/d ratios were larger than 2.4. The ETS strengthening system in the beam with a/d = 2.4 is the most effective strengthening.
- The proposed analytical model for estimation of maximum shear force of ETS-retrofitted beams and the shear resistance of ETS intervening system was rational and safe by broadly validating the calculated results with the experimental and numerical data.
- In future studies, the effects of sustained loading and fatigue on ETS-FRP-strengthened beams, particularly under real-life service conditions, should be investigated through both experimental and numerical approaches. Additionally, sensitivity analyses of mesh size and shear transfer coefficients are necessary to ensure both accuracy and optimization in the numerical modeling of ETS-FRP-strengthened beams. Conversely, the simulation of the anchorage at the ends of each individual ETS-FRP rod, particularly in T-shaped strengthened beams, should be further investigated. The brittle failure of high-strength concrete beams with high ETS reinforcement stiffness is also an important issue that should be examined in future studies.

7. Declarations

7.1. Author Contributions

Conceptualization, L.V.H.B. and B.S.; methodology, L.V.H.B. and B.S.; software, L.V.H.B.; validation, L.V.H.B.; formal analysis, L.V.H.B. and B.S.; investigation, L.V.H.B. and B.S.; resources, L.V.H.B. and B.S.; data curation, L.V.H.B. and B.S.; writing—original draft preparation, L.V.H.B. and B.S.; writing—review and editing, L.V.H.B. and B.S.; visualization, L.V.H.B.; supervision, B.S.; project administration, L.V.H.B. and B.S.; funding acquisition, L.V.H.B. and B.S. All authors have read and agreed to the published version of the manuscript.

7.2. Data Availability Statement

The data presented in this study are available within the article.

7.3. Funding and Acknowledgments

This research project is supported by the Second Century Fund (C2F), Chulalongkorn University, Thailand. The first author acknowledges Ho Chi Minh City University of Technology (HCMUT), VNU-HCM for supporting this study.

7.4. Conflicts of Interest

The authors declare no conflict of interest.

8. References

- [1] Dias, S. J. E., & Barros, J. A. O. (2008). Shear Strengthening of T Cross Section Reinforced Concrete Beams by Near-Surface Mounted Technique. Journal of Composites for Construction, 12(3), 300–311. doi:10.1061/(asce)1090-0268(2008)12:3(300).
- [2] Rahal, K. N., & Rumaih, H. A. (2011). Tests on reinforced concrete beams strengthened in shear using near surface mounted CFRP and steel bars. Engineering Structures, 33(1), 53–62. doi:10.1016/j.engstruct.2010.09.017.
- [3] Chaallal, O., Mofidi, A., Benmokrane, B., & Neale, K. (2011). Embedded Through-Section FRP Rod Method for Shear Strengthening of RC Beams: Performance and Comparison with Existing Techniques. Journal of Composites for Construction, 15(3), 374–383. doi:10.1061/(asce)cc.1943-5614.0000174.
- [4] Le, A. T., Nguyen, T. N., & Van Cao, V. (2023). Bond-slip Behaviour of NSM GFRP Bars in Reinforced Recycled-Aggregate Concrete: Experiments and a Modified Model. Civil Engineering Journal (Iran), 9(2), 233–253. doi:10.28991/CEJ-2023-09-02-01.
- [5] Saadah, M., Ashteyat, A., & Murad, Y. (2021). Shear strengthening of RC beams using side near surface mounted CFRP ropes and strips. Structures, 32, 380–390. doi:10.1016/j.istruc.2021.03.038.
- [6] He, W., Wang, X., Monier, A., & Wu, Z. (2020). Shear behavior of RC beams strengthened with side-bonded BFRP grids. Journal of Composites for Construction, 24(5), 04020051. doi:10.1061/(ASCE)CC.1943-5614.0001069.
- [7] Oudah, F., & Petrie, C. (2025). Reliability-Based Design Aid for Evaluation and FRP Retrofit of Existing RC Bending Members by Considering Project-Specific Conditions. Journal of Composites for Construction, 29(3), 04025020. doi:10.1061/jccof2.cceng-4913.
- [8] Leaman Smith, A., Ross, B. E., Cousins, T. E., Ziehl, P., & K. C., L. (2025). Evaluation of Two Strengthening Methods for Rural Short-Span Precast Concrete Bridges in South Carolina. Journal of Structural Design and Construction Practice, 30(1), 04024084. doi:10.1061/jsdccc.sceng-1311.
- [9] Cao, V. Van. (2025). Effects of CFRP U-Wraps on the Behavior of NSM GFRP Retrofitted Reinforced Concrete Beams. Journal of Composites for Construction, 29(1), 04024087. doi:10.1061/jccof2.cceng-4884.
- [10] Djamaluddin, R., Irmawaty, R., Fakhruddin, & Yamaguchi, K. (2024). Flexural Behavior of Repaired Reinforced Concrete Beams Due to Corrosion of Steel Reinforcement Using Grouting and FRP Sheet Strengthening. Civil Engineering Journal (Iran), 10(1), 222–233. doi:10.28991/CEJ-2024-010-01-014.
- [11] Nassif, N., Talha Junaid, M., Maalej, M., Altoubat, S., & Barakat, S. A. (2024). Durability of Fiber-Reinforced Polymer (FRP) Bars: Progress, Innovations and Challenges Based on Bibliometric Analysis. Civil Engineering Journal (Iran), 10, 136–173. doi:10.28991/CEJ-SP2024-010-09.
- [12] Bui, L. V. H., & Stitmannaithum, B. (2020). Prediction of shear contribution for the FRP strengthening systems in RC beams: A simple bonding-based approach. Journal of Advanced Concrete Technology, 18(10), 600–617. doi:10.3151/JACT.18.600.
- [13] Breveglieri, M., Aprile, A., & Barros, J. A. O. (2014). Shear strengthening of reinforced concrete beams strengthened using embedded through section steel bars. Engineering Structures, 81, 76–87. doi:10.1016/j.engstruct.2014.09.026.
- [14] Bui, L. V. H., Stitmannaithum, B., & Ueda, T. (2020). Experimental Investigation of Concrete Beams Strengthened with Embedded Through-Section Steel and FRP Bars. Journal of Composites for Construction, 24(5), 4020052. doi:10.1061/(asce)cc.1943-5614.0001055.
- [15] Valerio, P., Ibell, T. J., & Darby, A. P. (2009). Deep embedment of FRP for concrete shear strengthening. Proceedings of the Institution of Civil Engineers: Structures and Buildings, 162(5), 311–321. doi:10.1680/stbu.2009.162.5.311.
- [16] Mofidi, A., Chaallal, O., Benmokrane, B., & Neale, K. (2012). Experimental Tests and Design Model for RC Beams Strengthened in Shear Using the Embedded Through-Section FRP Method. Journal of Composites for Construction, 16(5), 540– 550. doi:10.1061/(asce)cc.1943-5614.0000292.

- [17] Breveglieri, M., Aprile, A., & Barros, J. A. O. (2015). Embedded Through-Section shear strengthening technique using steel and CFRP bars in RC beams of different percentage of existing stirrups. Composite Structures, 126, 101–113. doi:10.1016/j.compstruct.2015.02.025.
- [18] Breveglieri, M., Barros, J. A. O., Aprile, A., & Ventura-Gouveia, A. (2016). Strategies for numerical modeling the behavior of RC beams strengthened in shear using the ETS technique. Engineering Structures, 128, 296–315. doi:10.1016/j.engstruct.2016.09.027.
- [19] Bui, L. V. H., Stitmannaithum, B., & Jongvivatsakul, P. (2020). Comprehensive investigation on bond mechanism of embedded through-section fiber-reinforced polymer bars to concrete for structural analysis. Journal of Building Engineering, 29, 101180. doi:10.1016/j.jobe.2020.101180.
- [20] Bui, L. V. H., Stitmannaithum, B., & Ueda, T. (2020). Simulation of concrete beams strengthened by embedded through-section steel and GFRP bars with newly developed bond model. Journal of Advanced Concrete Technology, 18(7), 364–385. doi:10.3151/jact.18.364.
- [21] Bui, L. V. H., & Nguyen, P. T. (2022). Shear strength model of the reinforced concrete beams with embedded through-section strengthening bars. Frontiers of Structural and Civil Engineering, 16(7), 843–857. doi:10.1007/s11709-022-0834-0.
- [22] Godat, A., Chaallal, O., & Neale, K. W. (2013). Nonlinear finite element models for the embedded through-section FRP shear-strengthening method. Computers and Structures, 119, 12–22. doi:10.1016/j.compstruc.2012.12.016.
- [23] ACI Committee 318. (2019). Building Code Requirements for Structural Concrete (ACI 318-19) and Commentary (ACI 318R-19). American Concrete Institute (ACI), Farmington Hills, United States.
- [24] ACI Committee 440.1R-15. (2002). Guide for the Design and Construction of Structural Concrete Reinforced with Firber-Reinforced Polymer (FRP) Bars. American Concrete Institute (ACI), Farmington Hills, United States.
- [25] JSCE. (1997). Recommendations for Design and Construction of Concrete Structures Using Continuous Fiber Reinforcing Materials, Japan Society of Civil Engineers (JSCE), Tokyo, Japan.
- [26] ANSYS. (2024). Finite Element Computer Software for Nonlinear Structural Analysis, Version 24R2. Canonsburg, , United States.
- [27] TIS20-2543. (2000). Steel Bars for Reinforced Concrete: Round Bars. TIS20-2543. Thai Industrial Standards Institute (TISI), Bangkok, Thailand. (In Thai).
- [28] TIS24-2548. (2003). Steel Bars for Reinforced Concrete: Round Bars. Thai Industrial Standards Institute (TISI), Bangkok, Thailand. (In Thai).
- [29] Hognestad, E., Hanson, N. W., & McHenry, D. (1955). Concrete Stress Distribution in Ultimate Strength Design. ACI Journal Proceedings, 52(12), 455–479. doi:10.14359/11609.
- [30] Willam, K. J., & Warnke, E. P. (1975). Constitutive Models for the Triaxial Behavior of Concrete. Proceedings of IABSE, Structural Engineering Report 19, Section III, 1-30.
- [31] Fédération Internationale du Béton (FIB). (2010). fib Model Code for Concrete Structures 2010. Lausanne, Switzerland.
- [32] Jirawattanasomkul, T., Dawei, Z., & Ueda, T. (2013). Prediction of the post-peak behavior of reinforced concrete columns with and without FRP-jacketing. Engineering Structures, 56, 1511–1526. doi:10.1016/j.engstruct.2013.05.049.
- [33] Leung, C. K. Y., Chen, Z., Lee, S., Ng, M., Xu, M., & Tang, J. (2007). Effect of Size on the Failure of Geometrically Similar Concrete Beams Strengthened in Shear with FRP Strips. Journal of Composites for Construction, 11(5), 487–496. doi:10.1061/(asce)1090-0268(2007)11:5(487).
- [34] Benzeguir, Z. E. A., El-Saikaly, G., & Chaallal, O. (2020). Size Effect of RC T-Beams Strengthened in Shear with Externally Bonded CFRP L-Shaped Laminates. Journal of Composites for Construction, 24(4), 04020031. doi:10.1061/(asce)cc.1943-5614.0001045.
- [35] Li, W., & Leung, C. K. Y. (2016). Shear Span–Depth Ratio Effect on Behavior of RC Beam Shear Strengthened with Full-Wrapping FRP Strip. Journal of Composites for Construction, 20(3), 04015067. doi:10.1061/(asce)cc.1943-5614.0000627.
- [36] Triantafillou, T. C. (1998). Shear strengthening of reinforced concrete beams using epoxy-bonded FRP composites. ACI Structural Journal, 95(2), 107–115. doi:10.14359/531.